JOURNAL OF PETROLOGY | VOLUME 52 | NUMBER 3 | PAGES 457–486 | 2011 | doi:10.1093/petrology/egq087

Fluid Migration above a Subducted Slab—Constraints on Amount, Pathways and Major Element Mobility from Partially Overprinted Eclogite-facies Rocks (Sesia Zone, Western Alps)

MATTHIAS KONRAD-SCHMOLKE[1]*, PATRICK J. O'BRIEN[1] AND THOMAS ZACK[2]

[1]UNIVERSITÄT POTSDAM, INSTITUT FÜR ERD- UND UMWELTWISSENSCHAFTEN, KARL-LIEBKNECHT-STRAßE 24, 14476 POTSDAM, GERMANY

[2]UNIVERSITÄT MAINZ, FACHBEREICH GEOWISSENSCHAFTEN, BECHERWEG 14, 55128 MAINZ, GERMANY

RECEIVED APRIL 14, 2010; ACCEPTED NOVEMBER 24, 2010
ADVANCE ACCESS PUBLICATION JANUARY 8, 2011

The Western Alpine Sesia–Lanzo Zone (SLZ) is a sliver of eclogite-facies continental crust exhumed from mantle depths in the hanging wall of a subducted oceanic slab. Eclogite-facies felsic and basic rocks sampled across the internal SLZ show different degrees of retrograde metamorphic overprint associated with fluid influx. The weakly deformed samples preserve relict eclogite-facies mineral assemblages that show partial fluid-induced compositional re-equilibration along grain boundaries, brittle fractures and other fluid pathways. Multiple fluid influx stages are indicated by replacement of primary omphacite by phengite, albitic plagioclase and epidote as well as partial re-equilibration and/or overgrowths in phengite and sodic amphibole, producing characteristic step-like compositional zoning patterns. The observed textures, together with the map-scale distribution of the samples, suggest open-system, pervasive and reactive fluid flux across large rock volumes above the subducted slab. Thermodynamic modelling indicates a minimum amount of fluid of 0·1–0·5 wt % interacting with the wall-rocks. Phase relations and reaction textures indicate mobility of K, Ca, Fe and Mg, whereas Al is relatively immobile in these medium-temperature–high-pressure fluids. Furthermore, the thermodynamic models show that recycling of previously fractionated material, such as in the cores of garnet porphyroblasts, largely controls the compositional re-equilibration of the exhumed rock body.

KEY WORDS: *fluid migration; subduction; fluid–rock interaction; Sesia Zone*

INTRODUCTION

The migration of aqueous fluids and the associated major- and trace-element transport in metamorphic rocks, and particularly in subduction zones, has been a topic of intense research in the last two decades (e.g. Poli & Schmidt, 1997; Bebout *et al.*, 1999; Scambelluri & Philippot, 2001; Manning, 2004; Zack & John, 2007). Migrating fluids released from the subducted slab as a result of devolatilization of hydrous minerals are responsible for mantle metasomatism, the production of subduction-related magmatic activity (e.g. Schmidt &

*Corresponding author. Present address: Universität Potsdam, Institut für Geowissenschaften, Karl-Liebknecht-Strasse 24–25, 14476 Golm, Germany. E-mail: mkonrad@geo.uni-potsdam.de

Poli, 1998) and the formation of large ore deposits (e.g. Rosenbaum *et al.*, 2005), as well as for triggering earthquake ruptures (e.g. Hacker *et al.*, 2003), and thus are of scientific, economic and social relevance. Furthermore, slab-derived fluids are important carriers of major and trace elements as well as isotopic signatures that contain encoded information about subduction-related processes in the downgoing slab, in the mantle wedge and in the lower crust (e.g. Ryan *et al.*, 1995; Sorensen *et al.*, 1997; Spandler *et al.*, 2003, 2007; Kessel *et al.*, 2005; Bouvier *et al.*, 2008).

It is evident, however, that depending on the mode of fluid transport (e.g. pervasive or channelized) the migrating fluids interact differently with the wall-rocks during their ascent; however, in any case, fluid–rock interaction will lead to significant compositional modification of both the wall-rocks and the percolating fluids. Such fluid–rock interaction is often evident in exhumed high-pressure (HP) and ultrahigh-pressure (UHP) metamorphic rocks as an incomplete retrogression and re-hydration of primarily anhydrous eclogite-facies mineral assemblages (e.g. Schulte & Sindern, 2002). Several recent studies have revealed the existence of a narrow, highly strained mixing zone, often called the 'subduction channel', between the subducted slab and the overlying mantle wedge (e.g. Lin *et al.*, 1999; Bebout & Barton, 2002); this is most probably the site of syn-convergence exhumation of deeply subducted material (e.g. Escher & Beaumont, 1997). Within this zone, syn-kinematic fluid infiltration into metastable hot and dry (U)HP rocks on an exhumation path leads to a significant modification of wall-rock and fluid chemistry (e.g. Bebout & Barton, 1993). Thus, fluids released from the subducted slab are probably modified during their ascent within such a highly reactive subduction channel, depending on the intensity of rock deformation, the composition and amount of the infiltrated fluid, but also on reaction kinetics and permeability contrasts (Ague, 2007; Zack & John, 2007; van der Straaten *et al.*, 2008). It is evident that any information about processes in the subducted slab, which might have been recorded in the fluid properties, and fluid chemistry, becomes heavily modified during the interaction with rocks undergoing exhumation in the hanging wall of the downgoing plate. Therefore it is crucial to constrain the mode of fluid transport, to quantify the amount and composition of the infiltrated fluid and to understand the interplay between the infiltrated fluid and the wall-rock above the subducted plate.

Rock samples that interacted with metamorphic fluids and still partly preserve information about the pre-influx metamorphic stage are of greatest importance for the quantification of fluid fluxes and associated element cycling in subduction zones. In such partly reacted rocks the effect of fluid influx on the modes and compositions of newly formed or recrystallized phases can be directly observed and, if the thermodynamic response of the coexisting mineral paragenesis during fluid infiltration is known, constraints can be placed on the amount, composition and possibly the origin of the infiltrated fluid.

In this study we investigate four basic and felsic high-pressure metamorphic samples from the Western Alpine Sesia–Lanzo Zone (SLZ) that display excellent records of subduction zone fluid interaction with relatively dry wall-rocks at lower crustal and mantle depths. Fluid infiltration at blueschist-facies conditions during syn-convergent exhumation led to a partial compositional re-equilibration of hydrous high-pressure minerals, such as sodic amphibole and phengite, as well as to the formation of hydrous phases that partly replace the peak metamorphic eclogite-facies mineral assemblages.

To extract information about and to quantify the fluid–rock interaction from the compositionally zoned and newly formed minerals, we use various thermodynamic modelling techniques and compare modeled major element compositional trends and changing mineral paragenesis with those observed in our natural samples (see Konrad-Schmolke *et al.*, 2008*b*). We draw conclusions about the transport mode and amount as well as about the major element compositional effect of the infiltrating fluid on the wall-rock.

TECTONIC AND GEOLOGICAL SETTING

The Sesia–Lanzo Zone (SLZ) consists mainly of continent-derived rocks that were subducted to depths between 50 and 70 km during the Late Cretaceous (e.g. Dal Piaz *et al.*, 1972; Duchêne *et al.*, 1997; Rubatto *et al.*, 1999). Prior to subduction, the SLZ rocks occupied the distal part of the Apulian passive continental margin (e.g. Carraro *et al.*, 1970) and were separated from the European continental margin by the Early Jurassic Piemont–Liguria Ocean. Large parts of the SLZ rocks underwent Permian and Jurassic amphibolite- to granulite-facies metamorphism resulting in relatively dry rock compositions prior to subduction (e.g. Lardeaux & Spalla, 1991). The onset of convergence of the Apulian and European plates during the Cretaceous involved tectonic erosion and subduction of the SLZ rocks as well as subduction of the Piemont Ocean (e.g. Handy & Oberhänsli, 2004, and references therein). During convergence, the SLZ was exhumed in the hanging wall of the subducted oceanic plate prior to continent–continent collision (Babist *et al.*, 2006) and incorporated in the accretionary wedge-like Western Alpine nappe pile (Fig. 1a), within which it forms today the structurally uppermost segment.

The SLZ primarily consists of three large coherent metamorphic rock units (Fig. 1): the Mombarone and the Bard units, which are affected by an Alpine metamorphic

HP overprint (Babist *et al.*, 2006), and the so-called II DK unit, which preserves mainly pre-Alpine granulite- and amphibolite-facies schists and gneisses, as well as several smaller lenses of gabbro and peridotite (e.g. Carraro *et al.*, 1970; Dal Piaz *et al.*, 1971). The internally only weakly deformed Mombarone Unit is separated from the other units by blueschist-facies mylonitic shear zones (e.g. Gosso *et al.*, 1979; Babist *et al.*, 2006; Fig. 1) and a band of Mesozoic metabasites and metacarbonates [Monometamorphic Cover Complex (MCC) of Venturini (1995)] that is interpreted to form the nappe separator between the internal Mombarone and the external Bard unit.

Predominant rock types of the Mombarone unit are felsic quartz-rich coarse-grained garnet–omphacite–sodic amphibole–paragonite–phengite ortho- and para-gneisses and schists (e.g. Rubie, 1983; Koons, 1986), basic coarse-grained garnet–omphacite–sodic amphibole–paragonite–epidote gneisses, smaller lenses of sodic amphibole-bearing basic eclogite and omphacite–phengite–zoisite-bearing marble, as well as subordinate quartzite and ultrabasic rocks (e.g. Compagnoni *et al.*, 1977; Castelli, 1991; Ferraris & Compagnoni, 2003). Peak metamorphic conditions in these rocks were about 500–600°C at pressures between 1·5 and 2·0 GPa (Pognante, 1989; Tropper *et al.*, 1999*z*; Zucali *et al.*, 2002). Blueschist-facies viscous deformation at the contact between the Mombarone and the Bard Units (Tallorno Shear Zone) affected felsic and basic rock types and led to well-equilibrated ± garnet-bearing albitic plagioclase–epidote–sodic amphibole–paragonite–phengite mylonites (e.g. Gosso *et al.*, 1979; Babist *et al.*, 2006). In the more external Alpine Bard Unit the greenschist-facies overprint is more pervasive, reflected in fine-grained albitic plagioclase–white mica–epidote–biotite gneisses with minor intercalations of chlorite–calcic amphibole gneiss and subordinate phengite-bearing quartzite. Alpine peak metamorphic conditions attained in the Bard Unit are estimated to have been 1·0–1·5 GPa at 500–550°C (Lardeaux & Spalla, 1991).

SAMPLES

We investigated four samples that were collected within the Mombarone Unit (Fig. 1b). The samples represent the two major rock types of the SLZ and can be divided into two chemically different groups: two samples are characterized by higher K, Al and Si concentrations, thus reflecting their felsic precursor, and two are characterized by high Ca, Na and Mg and lower K and Si contents, reflecting the more basic composition of the protolith. Representative examples of both felsic and mafic rocks types are described in greater detail below. Major and trace element bulk-rock compositions are given as Electronic Supplementary Material (available at http://www.petrology.oxfordjournals.org).

Mineral assemblages and mineral chemistry in samples MKS-52-1 and MKS-55-1

The weakly deformed samples are moderately foliated and fine- to medium-grained (Fig. 2). The weak foliation in the basic sample (MKS-52-1, Fig. 2a) is parallel to a compositional banding defined by garnet-, sodic amphibole-, quartz- and mica-rich layers. The metapelitic sample (Fig. 2b), containing sodic amphibole, white mica and omphacite (or pseudomorphs after omphacite) in a quartz-rich matrix, is more homogeneous with a moderate foliation defined by sodic amphibole and white mica. In both samples the foliation is interpreted to be syn-kinematic with respect to the mylonitic blueschist-facies shear zone at the contact between the Mombarone and Bard Units (see Babist *et al.*, 2006).

The samples have a high-pressure mineral assemblage, the oldest preserved stage, of quartz (predominant in the felsic sample) + phengitic white mica + omphacite + sodic amphibole + garnet + rutile + paragonite, with differences being restricted to variation in modal proportions. The felsic sample (MKS-55-1) is quartz- and mica-rich whereas the basic sample (MKS-52-1) is dominated by sodic amphibole, garnet and, if preserved, omphacite.

In all samples three major stages of retrograde metamorphic overprint associated with fluid influx are evident from the textural phase relations (Fig. 3). Each of the overprinting stages is preserved in the samples either in the form of compositional zonation in phengite and sodic amphibole or by the preservation of characteristic mineral assemblages (Table 1). The first two overprinting stages that occurred in the stability field of sodic amphibole are obvious in all samples, whereas the third, greenschist-facies overprint is only weakly developed and is restricted to a few areas in each thin section.

If preserved, the primary omphacite (cpx) forms grains up to 5 mm long, which commonly contain numerous inclusions of garnet, rutile and quartz. Compositional variations are only minor, ranging between Jd_{30} and Jd_{40} in the basic samples and between Jd_{50} and Jd_{60} in the felsic samples. The first retrograde compositional resetting of omphacite starts at the rims of large grains and produces patchy omphacite with lower jadeite content along a complex intra-grain network (Fig. 3a). In some places newly formed diopsidic omphacite overgrowths are found. In the next stage omphacite shows a characteristic and unusual replacement by pseudomorphs containing phengite, epidote, quartz and albitic plagioclase (Fig. 3b). The extent of the replacement and the amounts of replacement products vary within a single thin section. The relative amounts of pseudomorph phases vary from phengite-rich to albitic plagioclase-rich, but always with only small amounts of epidote (Fig. 3a and b). Interestingly, in some places epidote shows a topotactic replacement of the earlier

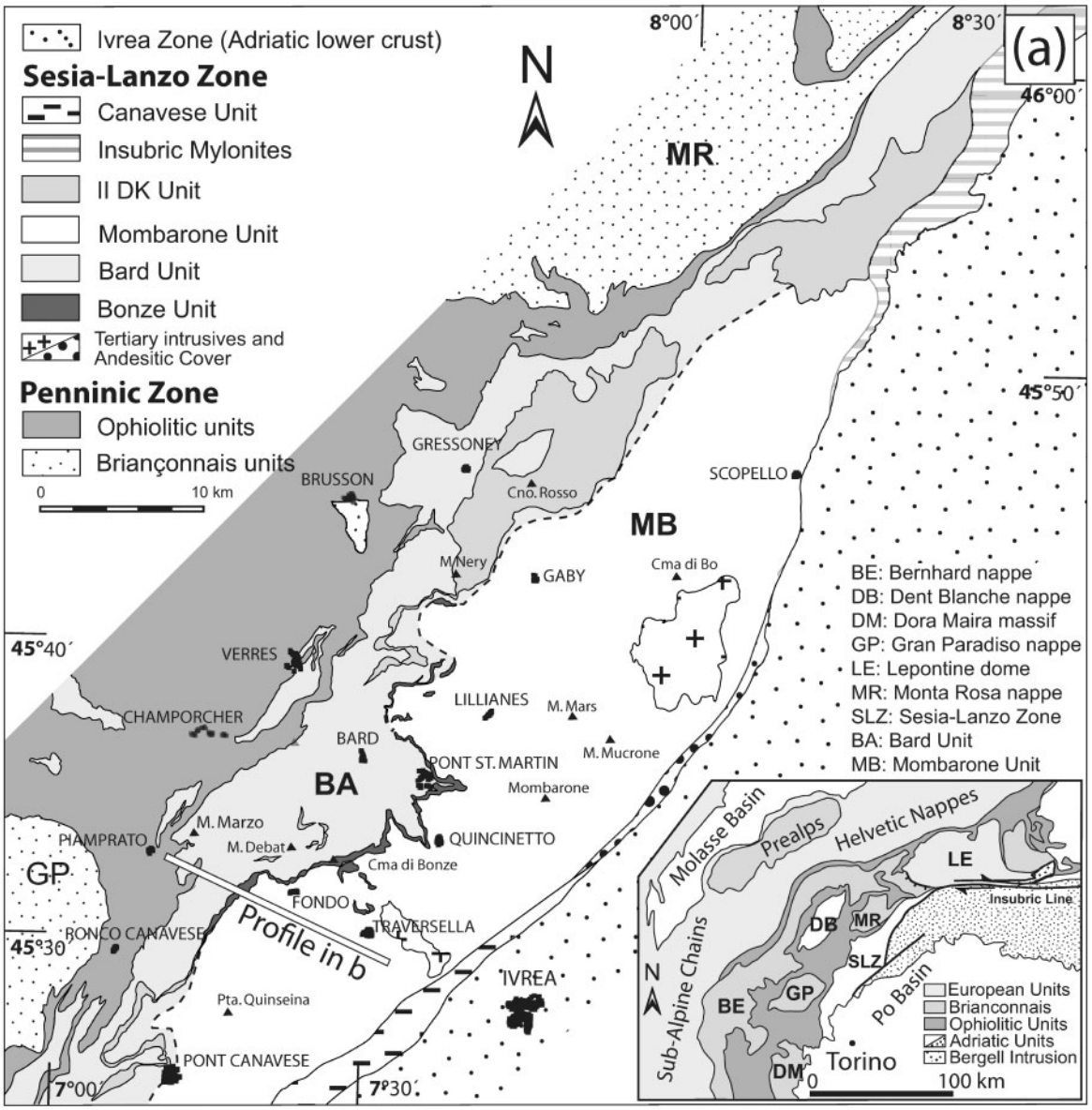

Fig. 1. (a) Simplified geological map of the Sesia–Lanzo Zone (SLZ) and adjacent areas. (b) Structural profile along the section shown in (a) and geological sketch representing the exhumation of the SLZ in Late Cretaceous time. Sample sites are along a transect across the Mombarone Unit. Figure modified from Babist *et al.* (2006).

pseudomorph texture, thus suggesting epidote growth after the phengite-bearing pseudomorph stage (Fig. 3b). Phengite in the pseudomorphs has lower Na but higher Fe than the cores of large matrix grains. Symplectite plagioclase is almost pure albite and epidote is zoned to slightly more Fe-rich rims. The third stage of omphacite modification is characterized by the formation of a finger-like vein network within the relict omphacite crystals that consists of sodic–calcic amphibole, mostly concentrated in the middle of the veins and sometimes arranged *en echelon*, and albitic plagioclase (Fig. 3a). None of the replacement textures show signs of a deformation after formation.

Primary phengite (phe) forms grains up to 3 mm long, in places intergrown with paragonite, and containing minor inclusions of garnet and quartz (Fig. 3). Primary phengite has between 3·3 and 3·5 Si per formula unit (p.f.u.), X_{Mg} between 0·6 and 0·7, and a slightly higher celadonite content in the basic samples. Chemical modification of phengite as a result of retrograde equilibration is visible in high-contrast back-scattered electron (BSE)

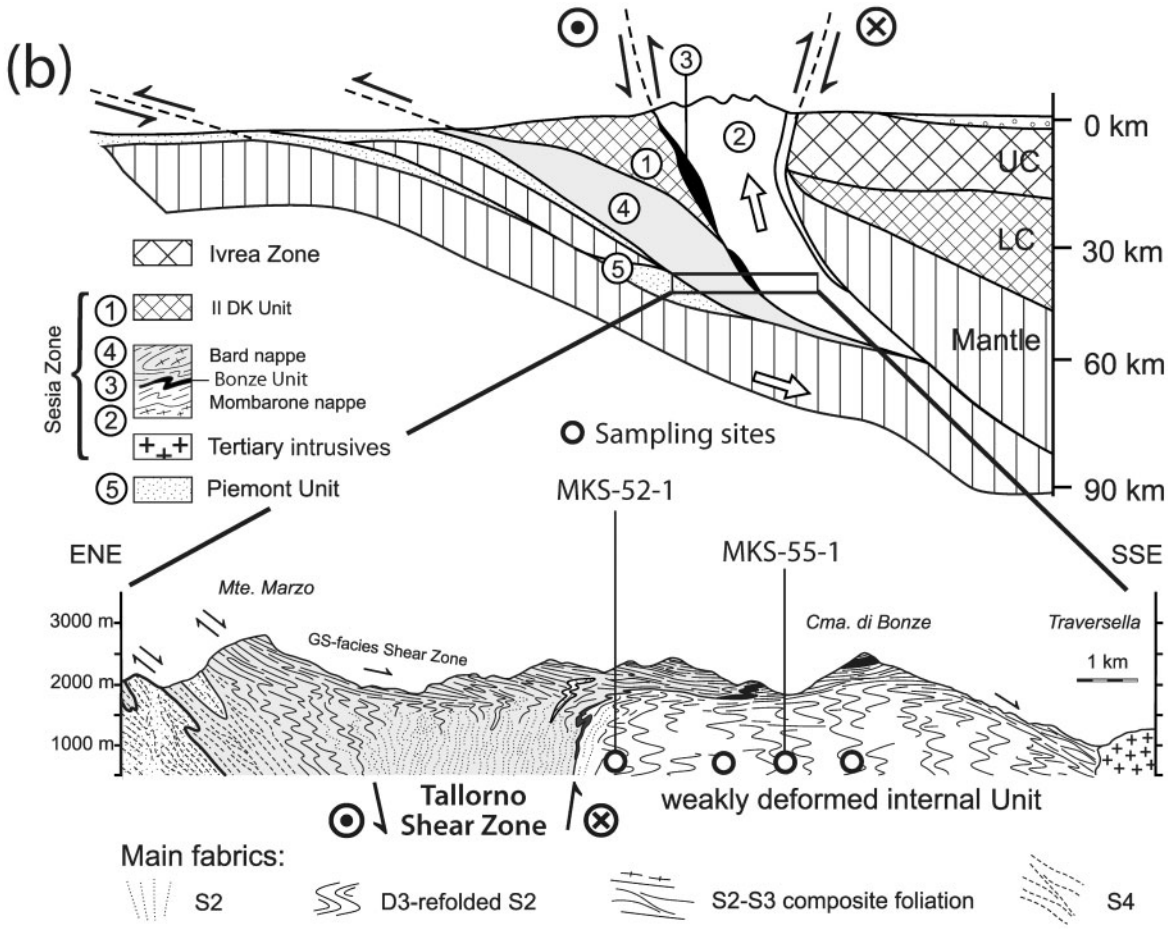

Fig. 1. Continued.

images (Fig. 3) and in compositional X-ray maps (Fig. 4). The BSE images show darker-coloured cores surrounded by brighter zones that are concentrated at the tips and grain boundaries (Figs 3c and 4a), around inclusions (Figs 3e and 4a) and in deformed parts (Fig. 3d) of many grains. The BSE images and X-ray maps reveal one, in some places two, different overprinting zones (Figs 3c and 4), which probably correspond to two different overprinting events. The boundary between unaffected and overprinted parts can be relatively sharp, but especially in deformed grains diffuse transitions also occur (Fig. 5b). The compositional variation between the homogeneous cores and the rims is mainly characterized by Fe–Mg exchange and an associated decrease in the X_{Mg} value (Figs 4b and 5b). A slight decrease in the Si content associated with an increase in tetrahedrally coordinated Al (Tschermak-substitution) is sometimes observable (Fig. 4c). Furthermore, overprinted areas are characterized by lower Na and Sr and higher Ba and Cl contents (Fig. 4). During the last overprinting event phengite is rimmed by biotite and oxide phases (Fig. 3).

Sodic amphibole (gln) grains, up to 5 mm long, commonly contain garnet, omphacite and quartz inclusions (Fig. 3). Primary sodic amphibole can be characterized as a solid solution between glaucophane and Fe-glaucophane with X_{Mg} between 0·55 and 0·7 (Fig. 5c). During initial retrogression sodic amphibole adjusts compositionally with a characteristic chemical trend in overgrowth zones as well as in intra-grain recrystallization and diffusion zones. The chemical modification of affected amphibole grains is reflected, in high-contrast BSE images, as a network of brighter (compared with the unaffected areas) amphibole material, varying in width and emanating from grain boundaries, brittle fractures and cleavage planes. The affected areas often have sharp boundaries towards the unaffected cores, but also more diffuse transitions between affected and unaffected parts occur. In the modified parts two, in places three, compositional variations can be observed. The first compositional overprint occurs only along grain boundaries, emanating mainly sub-parallel to the grain boundaries into the interior of the amphibole grains (Fig. 3f). It can be seen in weakly

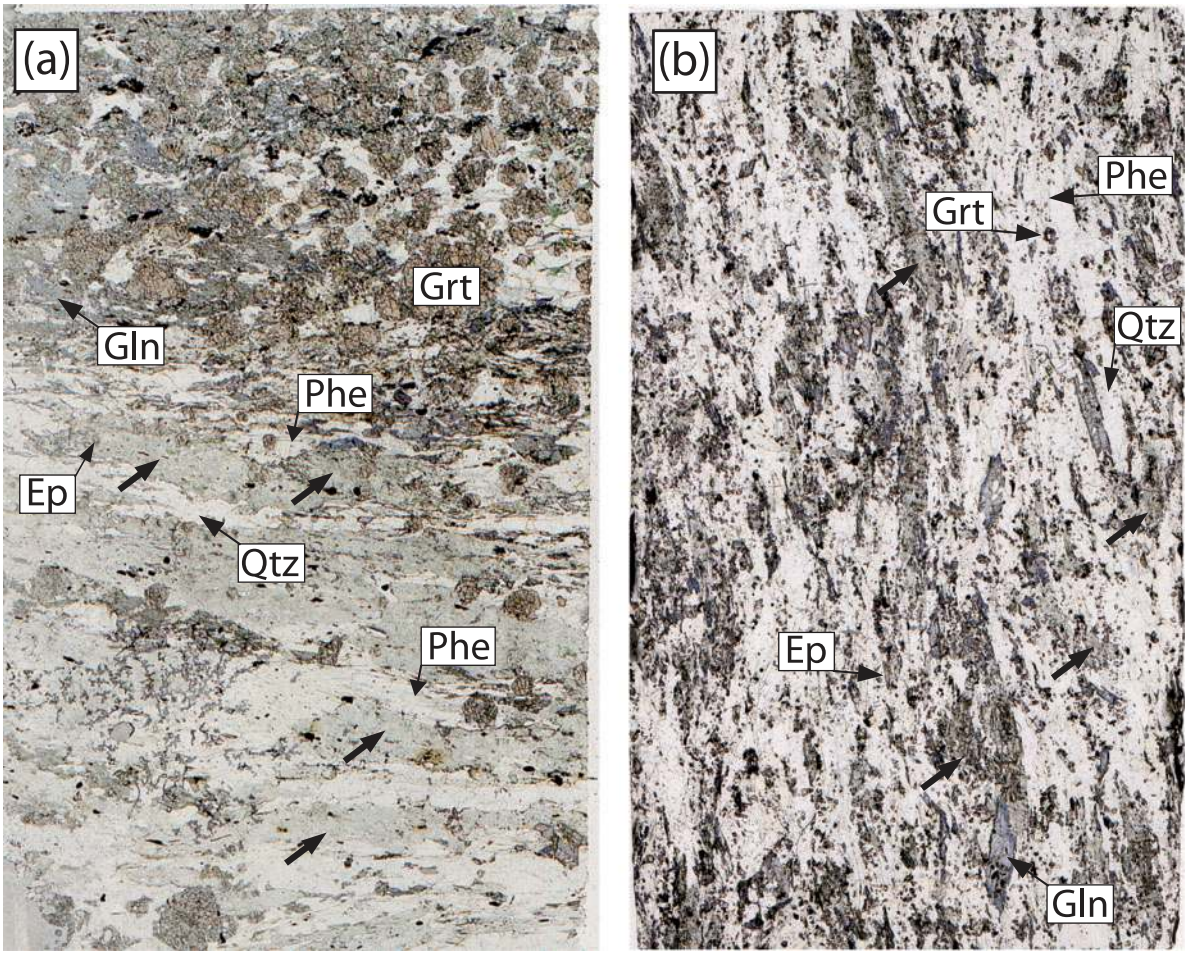

Fig. 2. Thin-section photographs of the selected samples. Both samples have similar phase assemblages but differ in modal amounts of the phases. (a) Sample MKS-52-1 has distinct compositional layering and a parallel, weak foliation. Within quartz-rich layers phengite–epidote–albitic plagioclase pseudomorphs after omphacite (bold arrows) are abundant. (b) The weakly foliated sample MKS-55-1 has also has a weak foliation, but a more homogeneous texture. Grt, garnet; Gln, sodic amphibole; Phe, phengite; Ep, epidote. Long side of the images is 4·5 cm.

retrogressed samples that this overprinting is related to the first retrograde metamorphic event, as modified sodic amphibole rims coexist with retrogressed omphacite. The second stage of overprinting is indicated by sodic amphibole with slightly brighter appearance in the BSE images; this has a more diffuse pattern although it seems to be concentrated along the grain boundaries (Fig. 3g). The third retrogression stage is characterized by the 'brightest' sodic amphibole composition and occurs mainly along brittle fractures that clearly postdate the two earlier overprint stages (Fig. 3g).

As in phengite, the compositional change across the boundary to the affected rims can be mainly characterized by Mg and Fe exchange (Fig. 4b). Mg contents change drastically and drop from values around 2·2 to 1·6 cations per formula unit (c.p.f.u.) followed by a further decreases to values around 1·45. The change in the Fe content is inverse with a sharp increase from 0·9 to 1·4 c.p.f.u. and a further increase towards the rim. Although Ca is a minor component it shows a slight increase, as does calculated tetrahedral Al, whereas octahedral Al shows a slight decrease towards the overprinting zones. Si and Na show no significant differences between cores and overprinted rims (Fig. 4c and d). In contrast to phengite, sodic amphibole in places exhibits oscillatory growth zonation (Fig. 3h).

The last retrogression of sodic amphibole is in some areas visible at the outermost rims of the amphibole grains, where it is often replaced by chlorite, calcic amphibole and albitic plagioclase, indicating a static greenschist-facies overprint (Fig. 3d and f).

The numerous idiomorphic to sub-idiomorphic, almost inclusion-free garnet (grt) grains vary in size from 50 to 200 μm in diameter and preserve compositional growth zonation (Fig. 5d). In most cases the variation is only a minor increase in Prp and X_{Mg} [$Mg/(Mg + Fe^{2+})$] associated with a decrease in Alm and Grs from core to rim.

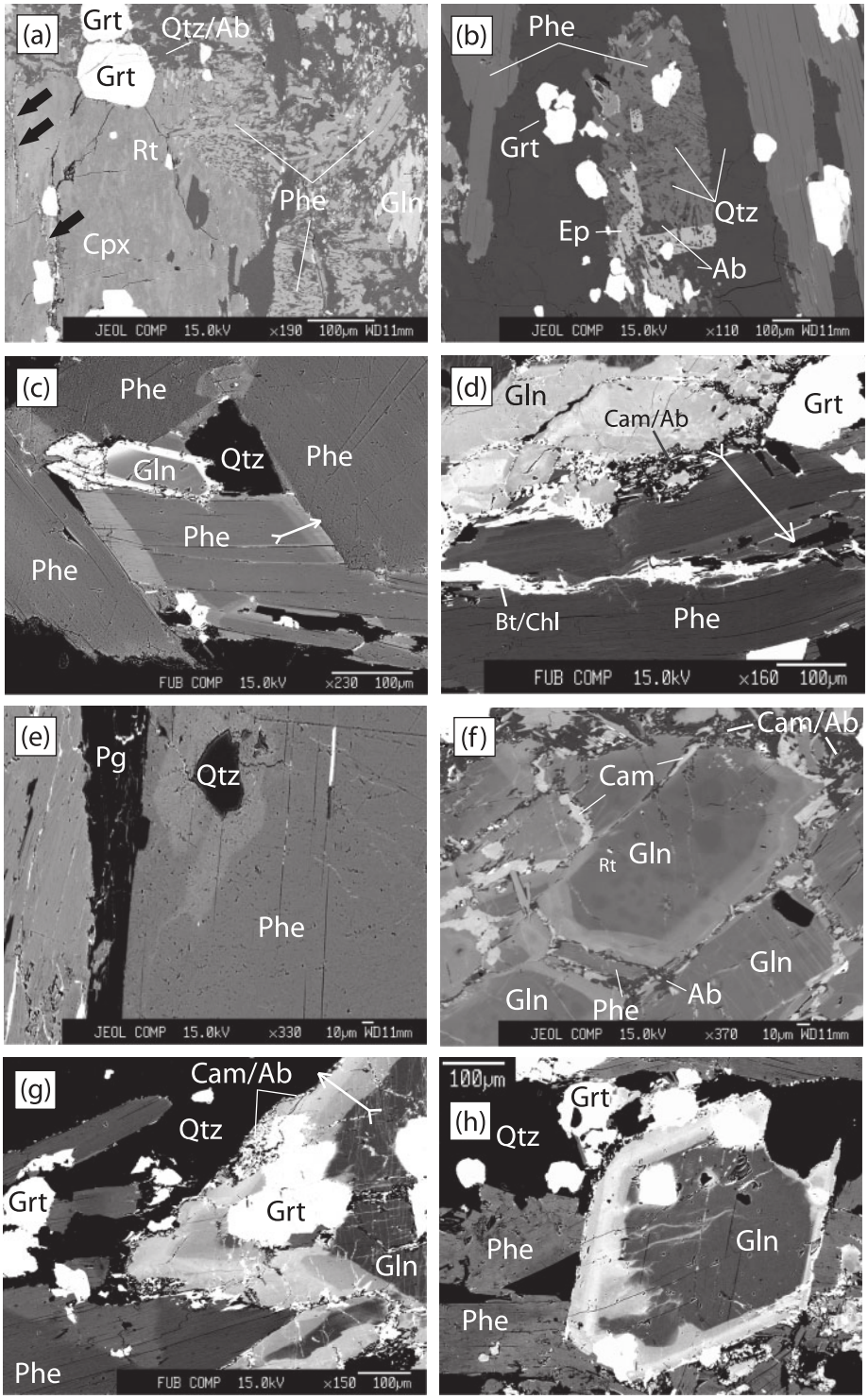

Fig. 3. Back-scattered electron images of minerals affected by the fluid influx. (a, b) Relict omphacite (Cpx) is compositionally modified and replaced by phengite, epidote, albitic plagioclase and, later, by calcic amphibole (arrows). (c–e) Phengite shows modified (brighter) areas along grain boundaries and deformed parts. (f–h) Overprinting features in sodic amphibole along fluid pathways, such as grain boundaries (f) and (g), microcracks (g) and (h), as well as overgrowth zones (h). (See text for further details.) Arrows in (d) and (g) indicate the positions of the compositional profiles in Fig. 5. Cam = calcic amphibole.

Table 1: Changing mineral assemblages in the samples at peak metamorphic conditions, during fluid influx and static greenschist-facies overprint

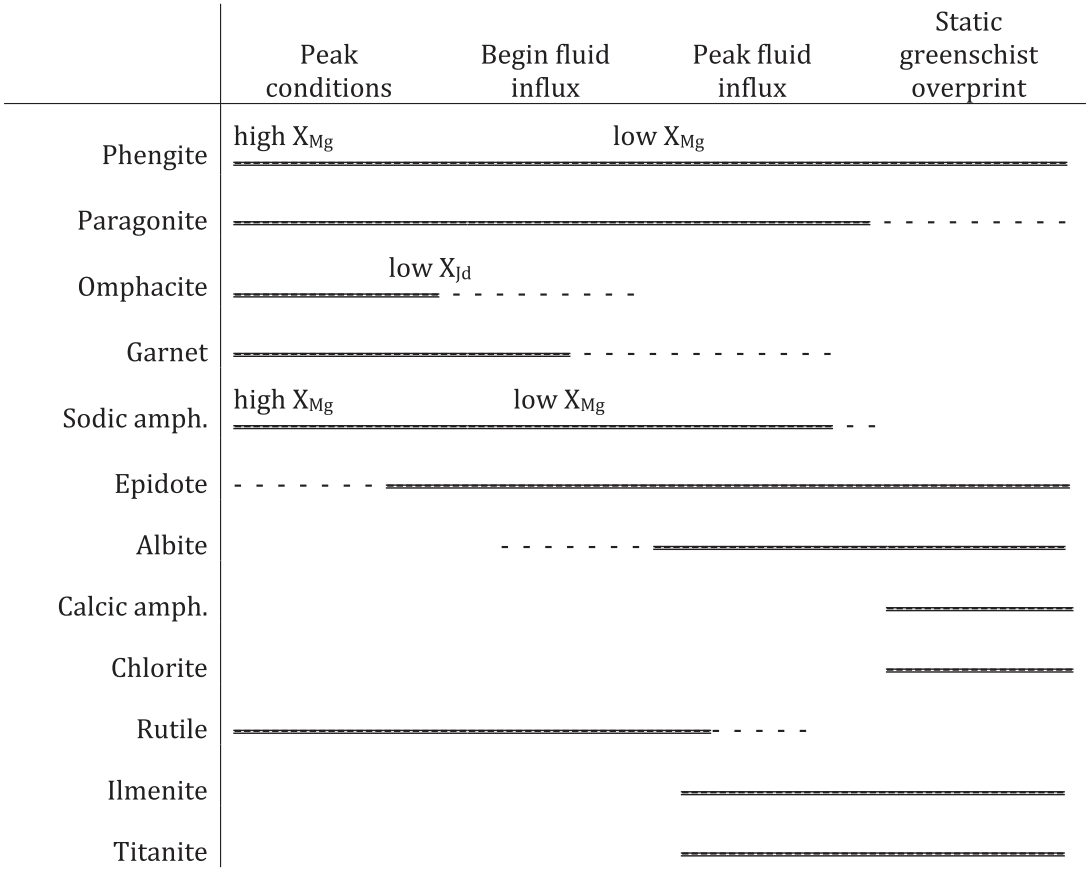

Sps content in all investigated garnets is low ranging from 1 to 10 mol %. Garnet shows signs of resorption, indicated by crosscutting relations between the grain boundary and zonation pattern, but without obvious replacement by other phases (Fig. 4h). In sample MKS-52-1 newly formed garnet, with higher Mn and lower Ca, overgrows the rims of large porphyroblasts and infiltrates the interior of the porphyroblasts along a sub-grain boundary networks (Fig. 4h; see Konrad-Schmolke *et al.*, 2007). The overgrowth zones are characterized by sharp compositional gradients towards the host grains. In the latest preserved metamorphic stage garnet is partly replaced by chlorite.

Paragonite (pg) occurs in all samples, either in mica-rich layers or associated, sometimes intergrown, with phengite (Fig. 3e). Paragonite is more abundant in the felsic samples, where it forms grains up to several hundreds of microns in size with uniform composition. In a few areas paragonite replacement by albitic plagioclase can be observed.

Epidote (ep) occurs in the matrix, as well as in pseudomorphs and aggregates together with phengite that replace omphacite. In the matrix epidote forms grains up to 300 μm that are mostly rounded, but sometimes occurs also as elongate grains parallel to the main foliation. Epidote in pseudomorphs and phengite–epidote aggregates is often hypidiomorphic and forms grains up to 200 μm. Epidote composition is uniform with X_{Ep} between 0·6 and 0·7.

Calcic amphibole (cam) occurs as small acicular grains that are often associated with chlorite and albitic plagioclase along the rims of sodic amphibole, as well as within relict omphacite grains (Fig. 3a and f). Chemically calcic amphibole is tremolite, sometimes magnesiohornblende; it commonly has moderate Na(A) between 0·1 and 0·15 c.p.f.u. and tetrahedral Al contents ranging between 0·25 and 0·35 c.p.f.u.

Textural relations indicate that rutile (rt) is the stable Ti phase at peak conditions in both rock types. Rutile is found as inclusions in garnet, where it occurs

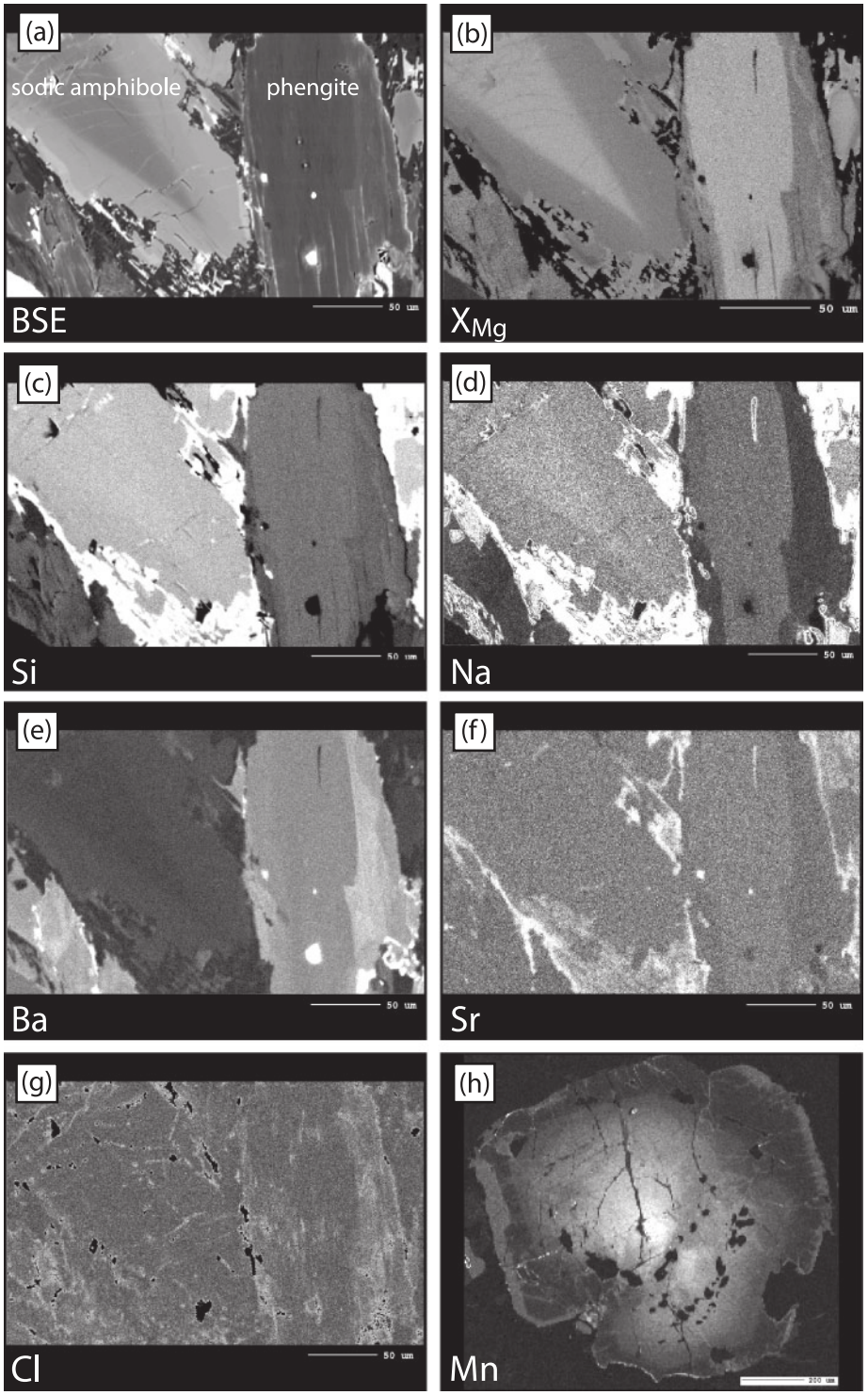

Fig. 4. (a–g) Back-scattered electron image (BSE) and compositional maps of sodic amphibole and phengite from sample MKS-55-1 (lighter shades in the compositional maps indicate higher concentrations). The BSE image (a) correlates inversely with the X_{Mg} pattern (b), which in turn mimics the compositional maps of Na (d) and Sr (f), all of which show significantly lower values along the rims. In contrast, the concentrations of Ba (e) and Cl (g) are higher in the overprinted rims than in the cores. Variations in Si (c) content are only minor in both phases. It should be noted that the Na map (d) is a composite image focusing on Na concentrations in sodic amphibole and phengite respectively. (h) Manganese variation in garnet showing a sharp, sometimes diffusive enrichment in the rim, along microcracks and subgrain boundaries, indicating garnet resorption, overgrowth and Mn back-diffusion.

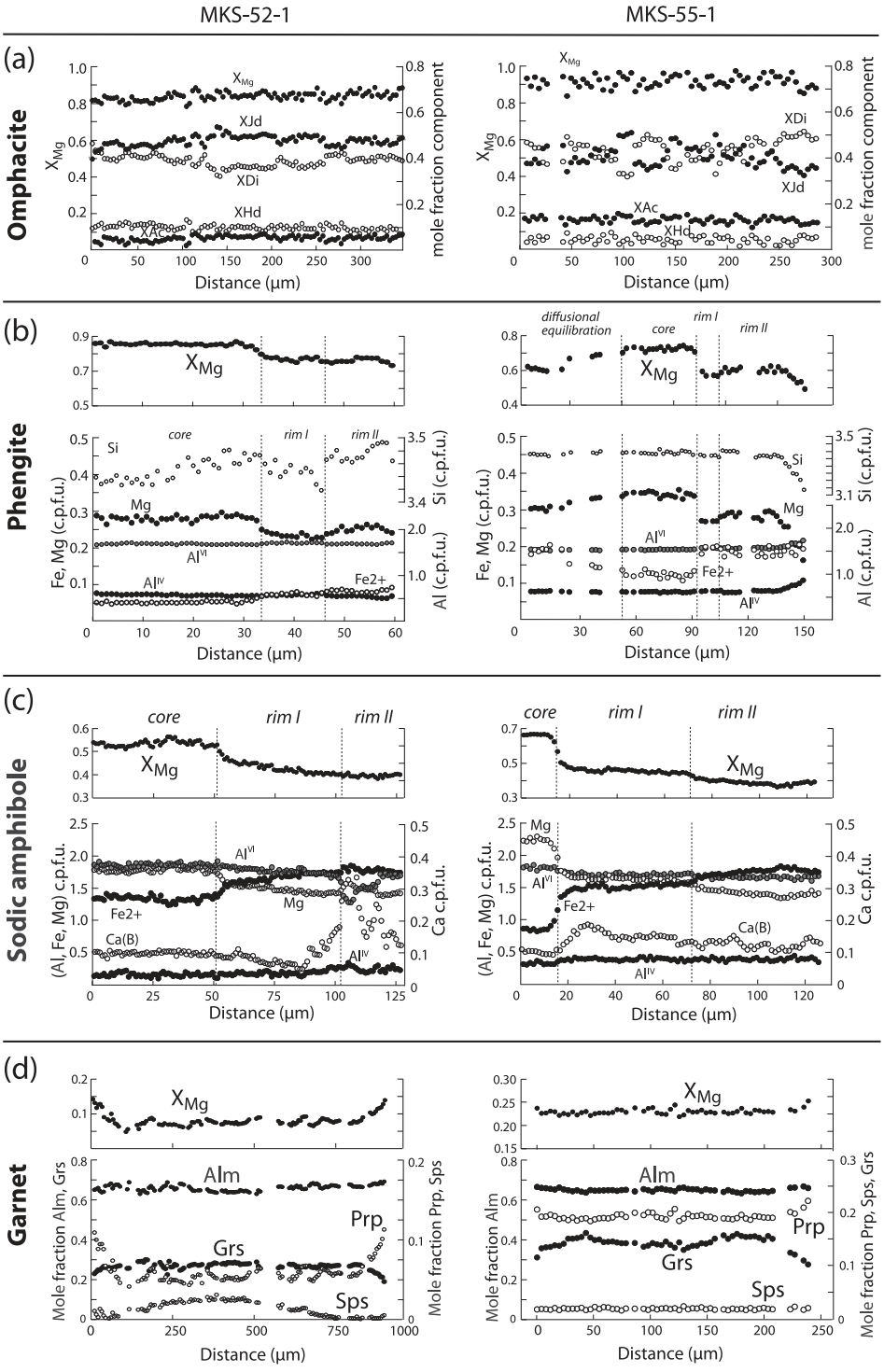

Fig. 5. Compositional profiles across representative grains of omphacite, phengite, sodic amphibole and garnet from samples MKS-52-1 and MKS-55-1. (a) Omphacite composition shows minor irregular variations without a clear core-to-rim trend. (b) The affected areas in phengite show a sharp shift towards more iron-rich compositions; other elements are largely unaffected. In deformed areas (left side of the profile) compositional transitions are smoother. (c) Sodic amphibole is also more iron-rich in the overprinted areas. Ca increases in some grains, but does not correlate with X_{Mg}. (d) Garnet preserves compositional growth zonation with a trend towards more Grs-poor and Prp-rich compositions at the rim.

predominantly in the outer cores and near the rims along with omphacite, sodic amphibole and phengite. Rutile has a grain size between 10 (small inclusions) and 200 μm (matrix grains aligned parallel to the foliation) and is generally more abundant in the basic than in the felsic samples. In the basic samples rutile is replaced by ilmenite along rims and cracks, whereas in the felsic samples rutile is overgrown by titanite.

In both rock types apatite and pyrite occur as accessory phases. Apatite is usually inclusion free and occurs in the matrix as well as inclusions in garnet. Apatite forms elongate roundish grains of up to 300 μm. Pyrite is more abundant in the basic samples than in the felsic ones and usually forms grains of up to 100 μm. Together with ilmenite, forming around rutile in the basic samples, pyrite is the major iron-rich accessory phase in the samples.

In summary, three retrogression stages control the paragenesis and mineral compositions in the samples (Table 1). The first retrogression drives omphacite, sodic amphibole and phengite rims to become more Fe-rich, whereas net transfer reactions are not evident. During the second retrogression omphacite is replaced by phengite–epidote–albitic plagioclase pseudomorphs, whereas sodic amphibole and phengite recrystallize and again shift towards more Fe-rich compositions. Garnet is resorbed and forms, together with omphacite, sodic amphibole and epidote. The last visible overprint produces calcic amphibole + albitic plagioclase from omphacite and calcic amphibole + chlorite + albitic plagioclase from sodic amphibole. During this stage garnet is replaced by chlorite, paragonite decomposes to albitic plagioclase, and phengite forms biotite. Electron microprobe analyses and calculated mineral compositions are included as Electronic Supplementary Data.

RELATION BETWEEN MINERAL ZONING AND *P–T–X* EVOLUTION

To correlate the growth and recrystallization zones in sodic amphibole and phengite with the pressure–temperature and chemical evolution, as well as to constrain the modal changes of stable solid and fluid phases, we calculated contoured P–T and P–$X\mathrm{H_2O}$ phase diagrams for the specific bulk-rock compositions of a basic (MKS-52-1) and a felsic (MKS-55-1) sample. Additionally, to constrain fluid input and output, as well as the effect of fractional crystallization on the phase assemblage, we performed thermodynamic forward modelling along a specified P–T path representing the metamorphic evolution of the SLZ (Babist *et al.*, 2006, and references therein). In contrast to isochemical phase diagrams, such forward models are suitable for modelling non-isochemical metamorphic rock evolution.

Forward modelling involved calculation of sample-specific thermodynamic properties at 25 P–T increments along the prograde segment of the P–T trajectory as well as at 100 increments along the retrograde branch (see arrow in Fig. 6). We used Gibbs' energy minimization, and modification of the effective bulk-rock composition between two P–T increments according to the amount of elements incorporated in those phases that are assumed to undergo fractional crystallization (garnet) or that are assumed to enter or leave the system (water) using the THERIAK algorithm (De Capitani & Brown, 1987; Konrad-Schmolke *et al.*, 2005, 2006). Further details, such as solid solution formulations and bulk-rock chemistries used in the models, are given in the Electronic Supplementary Data. To validate model settings we compare modelled major element compositional changes in garnet, sodic amphibole and phengite with the actual, measured compositional changes in these phases. The thermodynamic models were applied for different boundary conditions of the fluid budget during subduction and subsequent exhumation, based on naturally occurring situations.

On the prograde path we assume that any fluid liberated during dehydration reactions leaves the (rock) system. Garnet undergoes fractional crystallization and elements incorporated into the stable amount of garnet are removed from the effective bulk-rock composition (EBC). On the retrograde branch of the P–T trajectory the effects of two different processes on the samples are modelled: (1) the effect of water-fractionation, water undersaturation and re-hydration on the samples; (2) the effect of refractory garnet material being recycled into the EBC or staying isolated without thermodynamically equilibrating with the EBC.

Modelling results

Figure 6 shows the calculated phase relations in P–T diagrams for two selected samples (MKS-52-1 and MKS-55-1) in the temperature and pressure range of interest (a), as well as contours for the amount of water in the stable solid phases (b) and for X_{Mg} in sodic amphibole (c) and phengite (d). The stability fields of the observed coexisting phase assemblages in our samples are indicated by the shaded areas in Fig. 6a. Although different in detail, the phase diagrams for the two samples show broadly similar topologies.

At peak conditions (*c.* 2·0 GPa at 550°C) the equilibrium assemblage in both samples is predicted to contain garnet + omphacite + sodic amphibole + phengite + quartz. Paragonite is calculated to be stable at peak conditions in sample MKS-55-1 (Fig. 6a). The large multivariant stability fields are constrained by the zero mode lines of lawsonite and plagioclase, which are absent in the observed assemblage, and by the stability of omphacite, which was stable at peak conditions. The retrograde path of the P–T

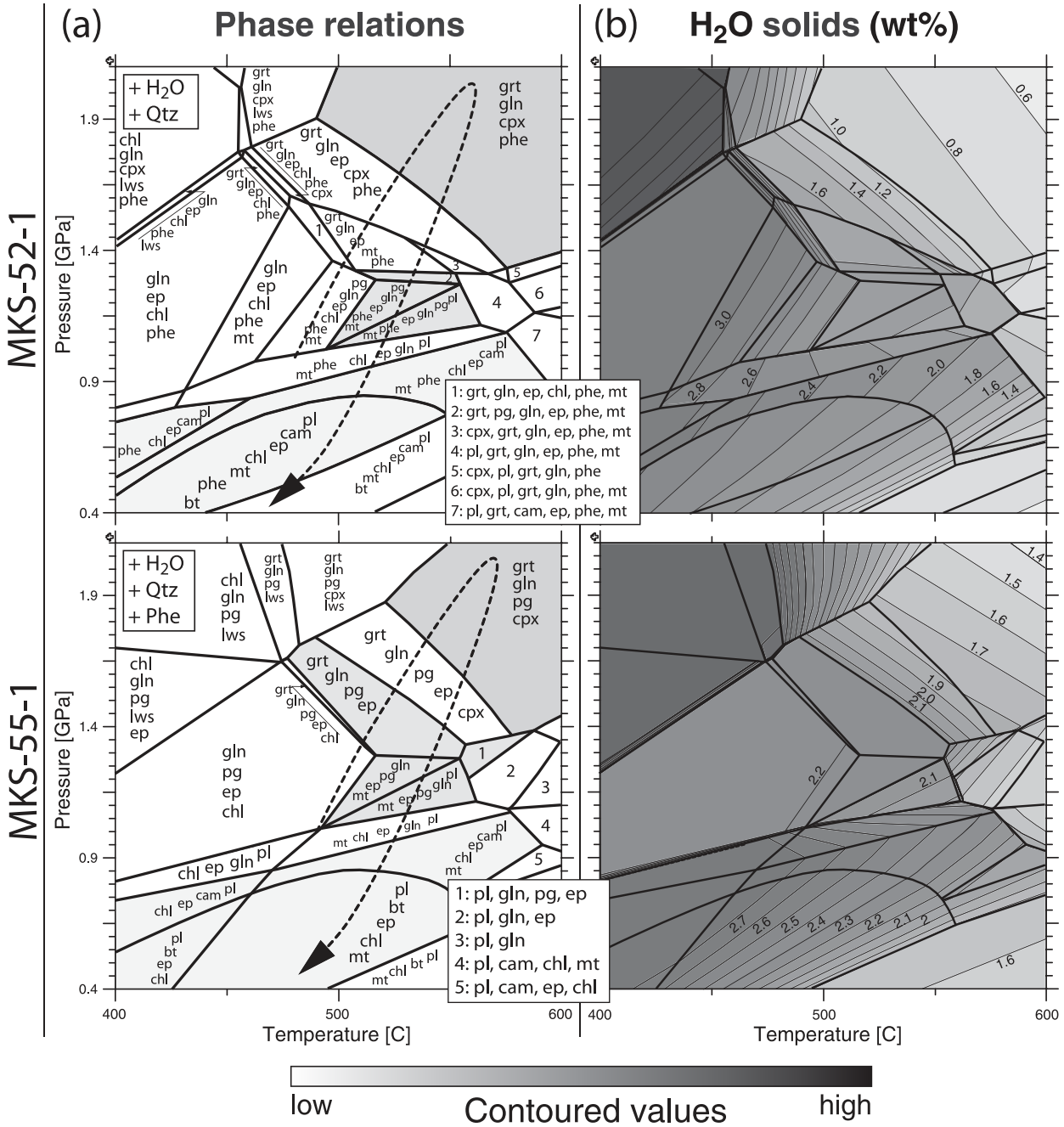

Fig. 6. *P–T* diagrams calculated for the bulk-rock compositions of the two samples. (a) Phase relations labelled for each field. The shaded areas correspond to the three parageneses that represent different metamorphic overprinting stages preserved in the samples. (b) Contours for the water content in solids calculated for the same diagram. Stability fields correspond to those in (a). (c) Contours for X_{Mg} in sodic amphibole are sub-parallel to those in (b), but show an inverse correlation. (d) Contours for X_{Mg} in phengite have a similar pattern to those in sodic amphibole. The white stippled isopleths in (d) are calculated Si c.p.f.u. in phengite. The dashed arrow in (a) marks the *P–T* trajectory used for the thermodynamic forward models.

trajectory (arrow) crosses the stability fields of all the observed retrogressional mineral assemblages (shaded areas in Fig. 6a) in our samples.

An important feature of the metamorphic history of our samples is demonstrated by the isopleth patterns in these diagrams relative to the *P–T* path followed. The isopleths for the water content have a positive slope below 1·1 GPa and a negative slope at higher pressures. At peak conditions the basic and felsic rocks are predicted to contain *c.* 0·65 and 1·5 wt % water, respectively. Thus, it is possible

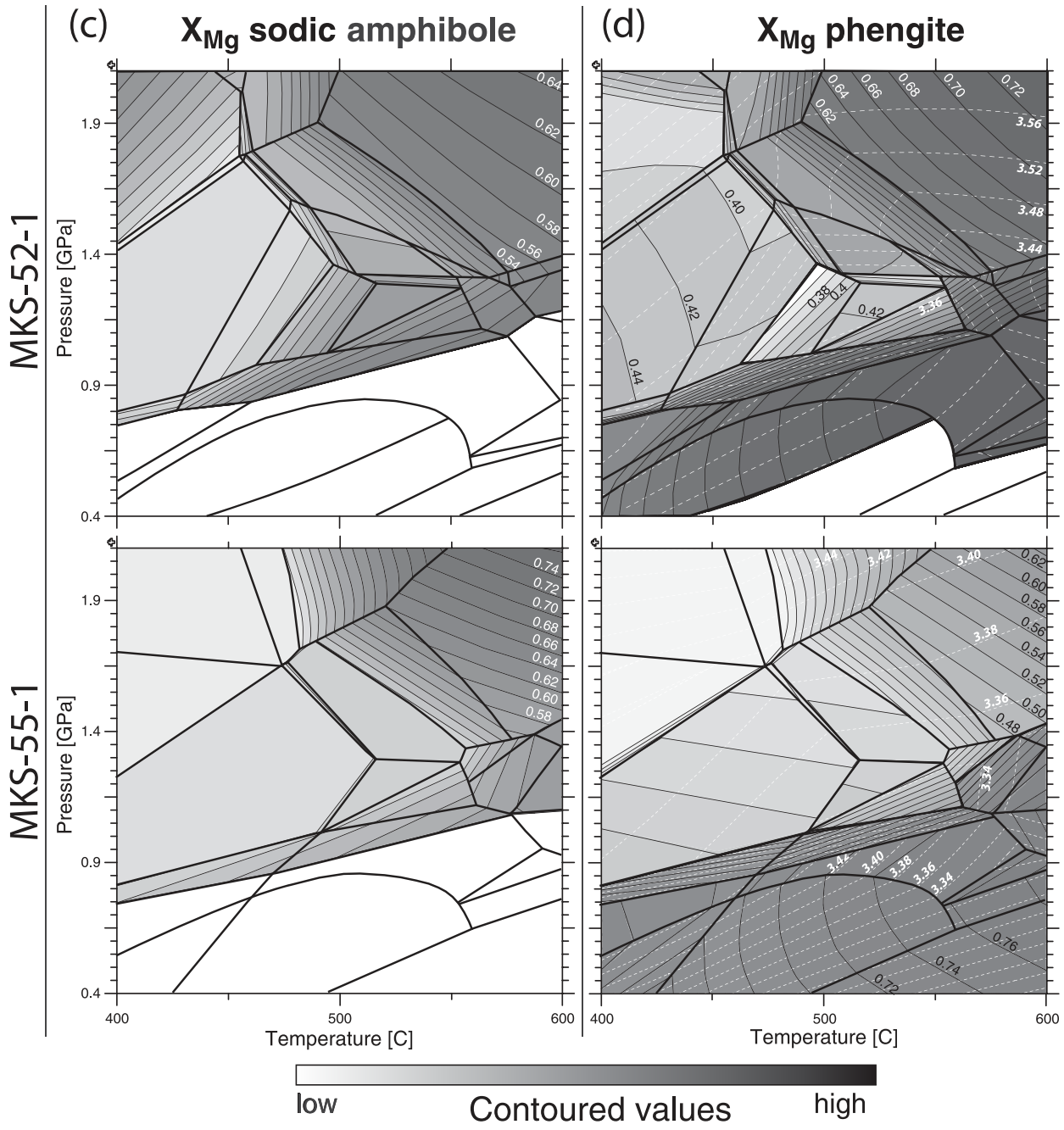

Fig. 6. Continued.

that decompression from the peak pressure, if not associated with a significant temperature increase, would result in water undersaturation of our samples if no external fluid was entrained above 1·1 GPa. The omphacite-free retrogressional mineral assemblage sodic amphibole + phengite + epidote ± garnet ± albitic plagioclase contains, at water saturation, about 1·8 wt % water in the case of the basic sample and about 2·2 wt % water in case of the felsic sample (Fig. 6b). Thus, to maintain water saturation and to produce the retrograde mineral assemblages observed in our samples a significant amount of water must have been added.

The X_{Mg} isopleths in amphibole (shown in Fig. 6c in those areas where the stable amphibole is sodic in composition) and phengite (Fig. 6d) lie sub-parallel to those for the water content but show an opposite pattern with

respect to the quantitative values. Whereas the calculated water content of our samples shows a characteristic increase along the retrograde branch of the P–T path associated with the formation of epidote and the breakdown of omphacite, the X_{Mg} patterns of amphibole and phengite are characterized by a large area with low X_{Mg} in both phases that extends from 400 to 550°C at 1·2 GPa in all diagrams. The X_{Mg} isopleths are closely spaced in those areas where amphibole coexists with clinopyroxene and/or plagioclase and are more widely spaced where sodic amphibole coexists with garnet and paragonite in the absence of omphacite and plagioclase. Generally, the isopleth patterns indicate a continuous decrease in the glaucophane component with decreasing pressure along the P–T trajectory up to 1·1 GPa. Comparing the calculated and observed compositional trends indicates that the Fe enrichment in amphibole and phengite of the natural samples is compatible with a decompression of the samples, although the calculated X_{Mg} values in phengite are slightly lower than those observed in the natural samples. In contrast to X_{Mg}, the calculated and observed Si contents in phengite (between 3·5 and 3·4 c.p.f.u. (cations per formula unit) in sample MKS-52-1 and MKS-55-1, respectively) are in agreement with postulated peak pressures between 1·8 and 2·0 GPa (Fig. 6d), and the widely spaced pattern of Si isopleths, especially in phase fields with coexisting paragonite (sample MKS-55-1), explains the minor silicon core-to-rim difference in the natural samples. However, it is evident that the step-like compositional zoning in the natural samples contradicts a continuous thermodynamic equilibration during exhumation.

The diagrams in Fig. 7 display the relation between modal changes in the phase assemblage (a), the compositional trends in phengite (b) and amphibole (c) as well as the water content and volume of solids (d) calculated along the retrograde segment of the P–T trajectory. Homogeneous equilibrium crystallization and water saturation are assumed. During the initial stages of the decompression, sodic amphibole, and in sample MKS-55-1 paragonite, is formed from omphacite and garnet. Around 1·5 GPa epidote also forms, which leads to a drastic decrease in the modal amount of omphacite and garnet, both of which are completely consumed at 1·3 GPa (Fig. 7a). These phase transitions are associated with a continuous X_{Mg} decrease in phengite and amphibole, which leads to a minimum X_{Mg} of around 0·5 between 1·4 and 1·2 GPa. This X_{Mg} minimum corresponds to the highest modal amounts of sodic amphibole in both samples. Amphibole consumption associated with the formation of plagioclase and/or magnetite leads to slightly increasing X_{Mg} in phengite and amphibole. The diagrams in Fig. 7d show, that, depending on bulk-rock chemistry, an influx of water of between 0·6 and 1·5 wt % is necessary to ensure water saturation of the samples along the decompression path. Depending on rock composition, decompression and rehydration are associated with up to a 17% volume increase that occurs in two stages in both samples (Fig. 7d). The eclogite- to blueschist-facies transition (between 1·4 and 1·2 GPa) is associated with 8 and 5% expansion in the basic and felsic sample respectively; the blueschist- to greenschist-facies transition contributes another 5% volume increase.

Nevertheless, the presence of large, compositionally zoned garnet porphyroblasts in both samples suggests fractional garnet crystallization during the prograde metamorphic evolution of the samples. As a consequence, the diagrams in Figs 5 and 6 might not correctly represent the crystallization sequence along the retrograde P–T segment, as they assume homogeneous equilibrium crystallization across the entire grid: a process contradicted by the occurrence of large garnet cores that are isolated from the EBC (see Marmo *et al.*, 2002; Konrad-Schmolke *et al.*, 2007). Furthermore, it is likely that water liberated during the prograde devolatilization of the samples left the rocks, which also might have influenced the crystallization history of the samples. To account for element fractionation along the prograde segment of the P–T trajectory we performed thermodynamic forward modelling under consideration of fractional garnet crystallization and water fractionation. The results of these models are shown in Fig. 8.

Prograde evolution

The diagrams in Fig. 8 show the modal abundances of the stable phases of interest (a) as well as the compositional evolution of phengite (b), amphibole (c) and garnet (d) calculated for the two chosen samples along the prograde branch of the P–T trajectory shown in Fig. 6. Both samples undergo significant dehydration, indicated by the significant decrease of hydrous phases and the increase of (accumulated) liberated water. Interestingly, dehydration occurs in two stages, one between 1·2 and 1·3 GPa and a second between 1·5 and 1·8 GPa, associated with the breakdown of chlorite, epidote and amphibole. The compositional evolution of phengite in both samples is characterized by an increase in the celadonite component, indicated by an increase in the Si content associated with a decrease in tetrahedral Al (Fig. 8b). This exchange is more pronounced in the basic sample. Additionally, X_{Mg} in phengite increases in both samples, a feature also more pronounced in the basic sample. In both samples X_{Mg} in amphibole changes towards higher values with increasing metamorphic grade. The Ca content of amphibole in both samples decreases slightly.

Garnet growth in both samples is connected with dehydration and the compositional change in garnet involves a continuous slight decrease in the almandine component associated with a slight increase of grossular and pyrope towards the inner rim (Fig. 8d). In the outer rim the

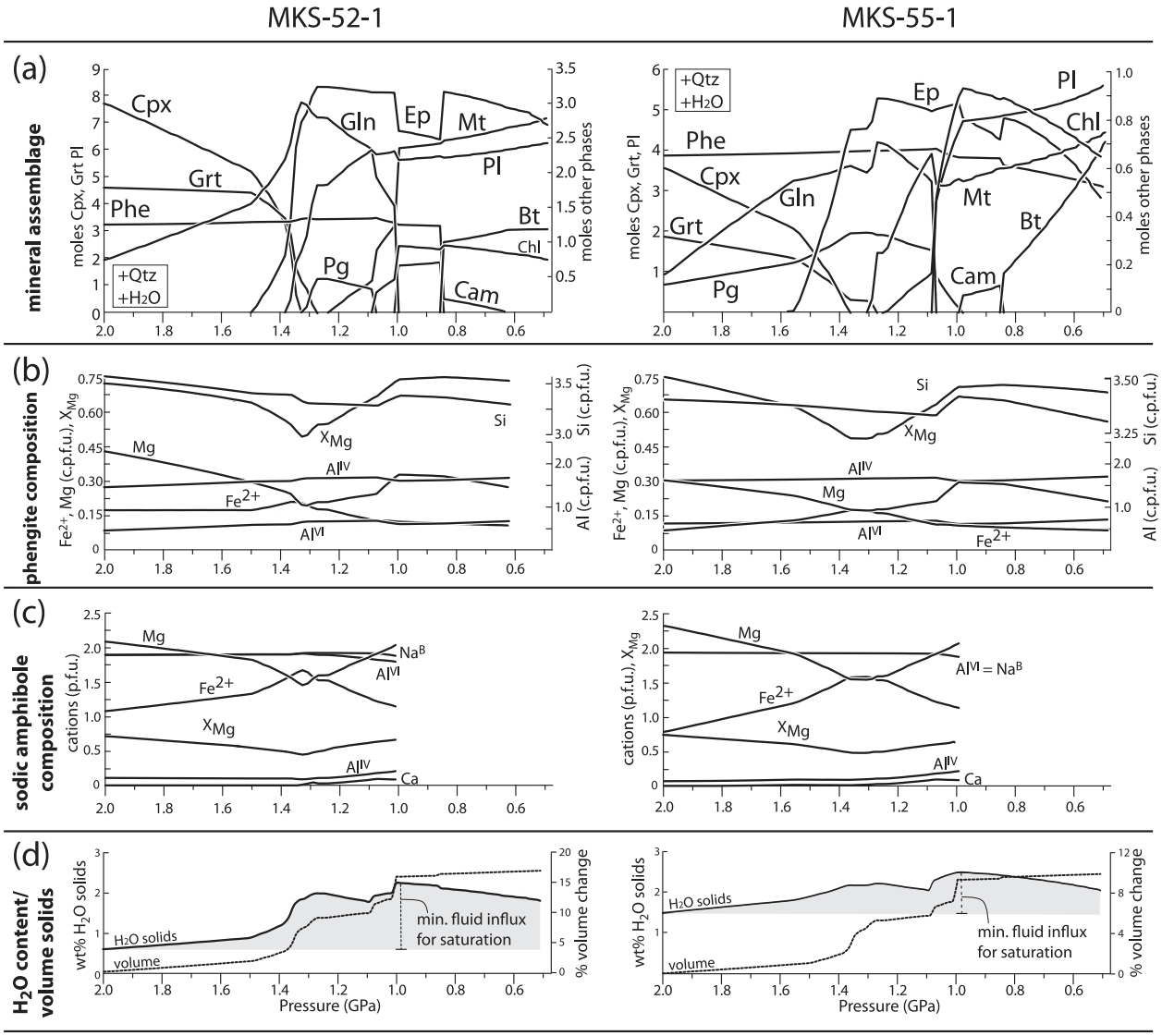

Fig. 7. Phase relations, phengite and amphibole compositions, water content and volumes of the solid phases calculated for the two samples along the retrograde segment of the P–T trajectory shown in Fig. 6. Homogeneous equilibrium crystallization and water saturation are assumed. The marked change in the phase assemblage between 1·6 and 1·3 GPa marks the transition from eclogite to blueschist facies associated with the formation of sodic amphibole and epidote and the breakdown of omphacite and garnet. The transformation is associated with a continuous decrease in X_{Mg} in phengite (b) and amphibole (c), which shows a characteristic minimum around 1·3 GPa. (d) The continuous increase of H_2O in the solids (bold continuous lines) indicates the need for water influx to maintain water saturation along the retrograde path. Rehydration and decompression is associated with a volume increase of 17 and 10% in the basic and felsic sample respectively (dotted lines).

trend changes and almandine and pyrope increase sharply, whereas grossular decreases. It is notable that the modelled trend in garnet chemistry correlates well with the observed compositional zoning in the garnet crystals in both samples (compare Figs 7 and 4), which in turn indicates a potentially good correlation between assumed and actual metamorphic evolution.

Fractional garnet crystallization and water liberation along the prograde P–T path significantly changes the EBC of the samples (see also Electronic Supplementary Data). Therefore, we calculated P–T pseudosections (Fig. 9a) as well as isopleths for the amount of H_2O in solid phases (Fig. 9b) and X_{Mg} in amphibole (Fig. 9c) for the chosen samples with the EBC at peak metamorphic conditions. Differences between the initial bulk-rock composition and the EBC used in these calculations are due to the fractional crystallization of garnet, which is present in our samples as compositionally zoned porphyroblasts, and due to the liberation of water during prograde dehydration reactions. This element fractionation led to a significant

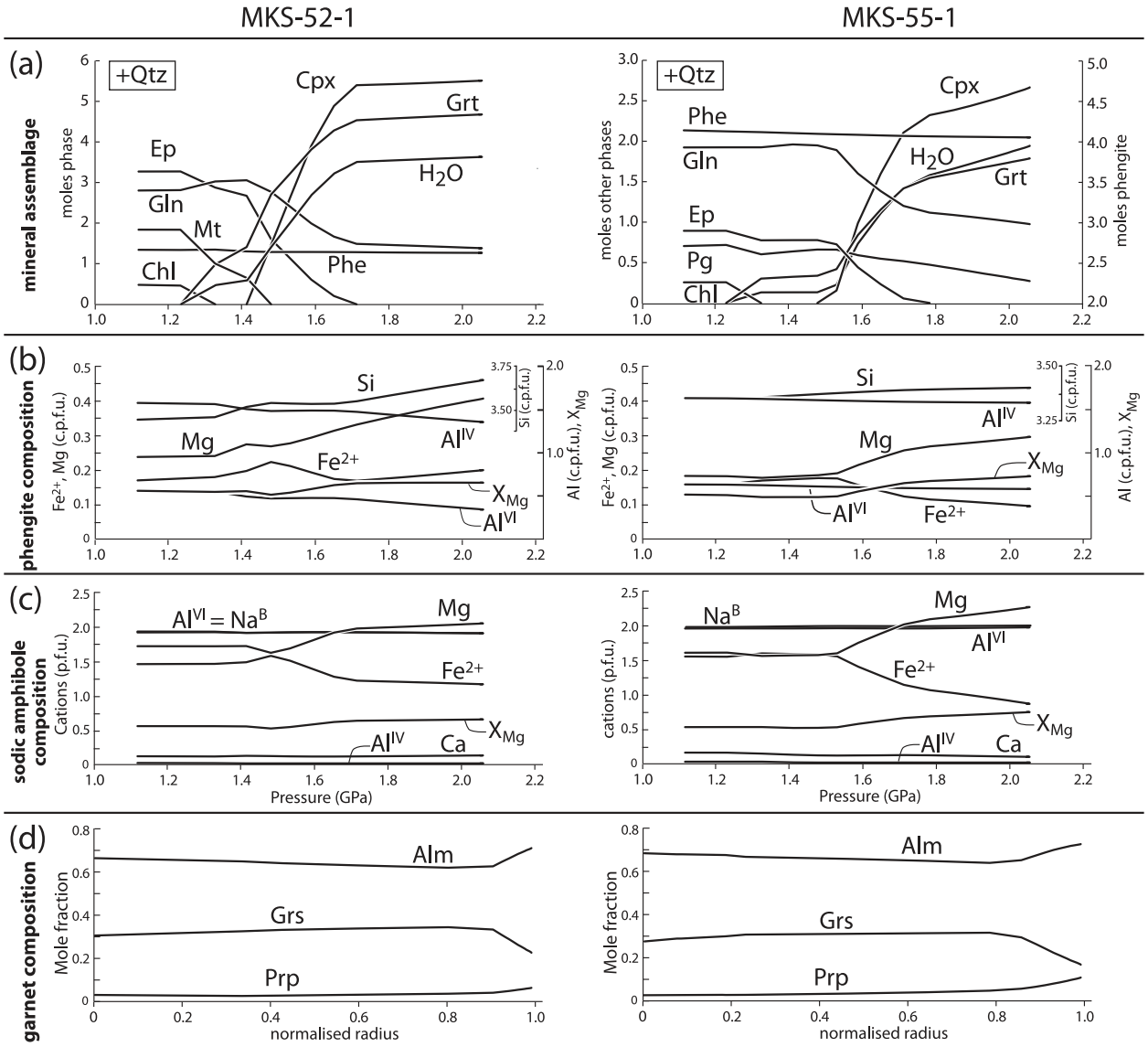

Fig. 8. Phase relations (a), phengite (b) and amphibole (c) compositions and the water content of the solid phases (a) calculated for the two samples along the prograde segment of the P–T trajectory shown in Fig. 6. Fractional garnet crystallization and release of liberated water are assumed. (a) Curves for the accumulated amount of water and garnet indicate two stages of dehydration and garnet formation. (b, c) Phengite and sodic amphibole become more Mg-rich with increasing pressure. (d) Garnet zonation patterns resemble those observed in the natural samples (see text).

modification of the phase topology compared with the diagrams in Fig. 6. It is, of course, notable that the P–T diagrams in Fig. 9 (like those in Fig. 6) are isochemical and do not reflect the effect of metasomatism during the rock's retrograde evolution, and thus are used only to demonstrate the potential effect of element fractionation on the retrograde metamorphic evolution.

The major differences in the phase relations between fractionated (Fig. 8) and unfractionated (Fig. 6) bulk-rock compositions are the restricted stabilities of epidote, chlorite and garnet, the absence of paragonite in the basic sample, as well as the enlarged stability field of omphacite in a fractionated EBC. Furthermore, the distance between the X_{Mg} isopleths for sodic amphibole is much larger and amphibole is generally more Mg rich. X_{Mg} in amphibole does not significantly change above the plagioclase stability boundary. In the large multivariant phase field of omphacite + sodic amphibole + phengite for sample MKS-52-1 and omphacite + sodic amphibole + phengite + paragonite for sample MKS-55-1, which

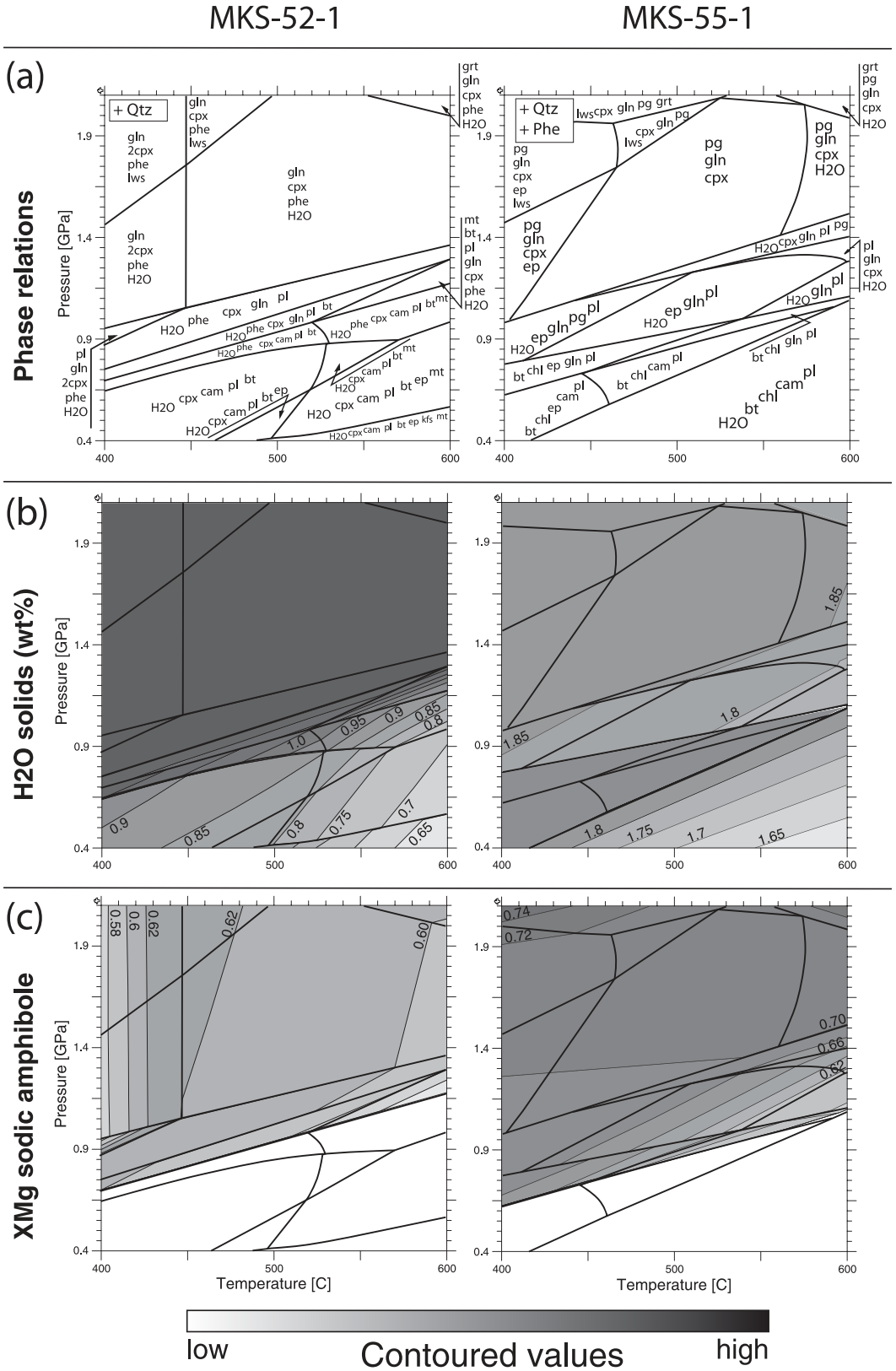

Fig. 9. *P–T* diagrams calculated for the effective bulk-rock compositions (EBC) of the two samples at peak metamorphic conditions (after fractional garnet crystallization and water release). (a) Phase relations, (b) contours for the water content of the stable phases and (c) contours for X_{Mg} in amphibole. Phase relations in (b) and (c) are as indicated in (a). It should be noted that water saturation (stable H_2O) is restricted owing to dehydration during prograde metamorphism. (See text for discussion.)

stretches across almost the entire upper half of the diagrams, X_{Mg} in amphibole varies only by 0·02 in both samples, with a minimum of 0·6 and 0·68 in the basic and felsic sample respectively. Thus, fractional garnet crystallization and water liberation have a significant influence on the composition of the coexisting phases. In the following sections we will demonstrate how this effect on amphibole and phengite can be used to reconstruct the evolution of solid and fluid phases during decompression of the samples.

Retrograde evolution

To study the influence of water infiltration on the amount and composition of stable phases during decompression we calculated isothermal P–$X\mathrm{H_2O}$ phase diagrams at 550°C for our samples (Figs 10 and 11). The diagrams in Fig. 10 are calculated for the unfractionated compositions of the samples; those in Fig. 11 are calculated for the EBC at peak metamorphic conditions. The diagrams show contours for X_{Mg} in amphibole (Figs 10b and 11b) and phengite (Figs 10c and 11c). Although these two-dimensional isothermal diagrams cannot fully display the retrograde evolution of our samples, as they ignore the assumed temperature decrease associated with the decompression, several important constraints on the rock evolution can be made.

The diagrams in Fig. 10 show that water saturation in the samples during decompression, assuming homogeneous equilibrium crystallization, can be attained only if significant amounts of water are added (see also Fig. 7d). Assuming the rock to be on the water saturation curve at peak conditions, which is likely if continuous dehydration occurred along the prograde path, the samples need between 1·5 and 1·0 wt % H_2O added to attain water saturation at lower pressures. Furthermore, the stability fields of epidote, omphacite, paragonite and garnet are strongly dependent on the water content. The same control accounts for sodic amphibole at very low water contents. In contrast, the occurrence of plagioclase is independent of the water content and is strongly pressure sensitive, even under water-undersaturated conditions. Interestingly, omphacite breakdown occurs at water-saturated conditions well above plagioclase stability, thus producing paragonite, epidote, garnet and/or sodic amphibole. At water-undersaturated conditions, omphacite breakdown coincides with plagioclase formation or occurs at lower pressures, thus predominantly producing plagioclase during decompression. This indicates that the reaction products of decomposing omphacite during decompression are dependent on the H_2O content of the rock, and might include (albitic) plagioclase, paragonite, epidote, garnet and sodic amphibole.

Particularly indicative of the water content of the samples are the X_{Mg} contents of amphibole and phengite. The X_{Mg} isopleths are near vertical in most water-undersaturated fields above plagioclase stability. The steep isopleths indicate that amphibole as well as phengite compositions at water-undersaturated conditions are very sensitive indicators for the addition of H_2O at any pressure. Increasing H_2O contents at elevated pressures cause significantly decreasing X_{Mg} values in these phases. Furthermore, the calculated X_{Mg} isopleths have contrasting orientations depending on the coexisting phases. A major change in the X_{Mg} isopleth patterns occurs if an iron- and/or aluminium-rich phase, such as garnet, epidote or magnetite, enters or leaves the mineral assemblage. This effect is visible in the diagrams in Figs 10 and 11, where the formation of epidote and magnetite in the basic and felsic sample, respectively, strongly deflects the X_{Mg} isopleths.

The effect on the composition of amphibole and phengite of the coexisting mineral assemblage is even more evident in a comparison of the P–H_2O diagrams calculated with and without fractionation effects (Figs 10 and 11). Figure 11 shows that as a result of fractional crystallization the stability of garnet, doubtless the most important Fe–Al phase in the rocks, is restricted to highly water-undersaturated conditions in both samples. In the presence of garnet + magnetite, most easily visible in case of the basic sample, the X_{Mg} isopleths are near horizontal, whereas those in the garnet- or magnetite-absent fields are subvertical or steeply dipping. Furthermore, X_{Mg} in amphibole and phengite is much higher, and the compositional variations in both phases are much smaller, in the diagrams calculated for the fractionated EBC, even at water-saturated conditions. However, the absence of magnetite in the natural samples is probably due to the fact that iron liberated by garnet and omphacite forms (apart from the X_{Mg} modification of phengite and amphibole) titanite, pyrite and epidote, whereas in the models, which do not consider Ti and S, partition of iron occurs mainly into epidote and magnetite.

Three retrograde evolution scenarios can be extracted from the P–H_2O diagrams: (1) homogeneous equilibrium crystallization without water re-saturation (i.e. the samples follow the red dotted line in Fig. 10b and c). This evolution implies complete equilibration of all minerals and recycling of previously fractionated garnet material into the EBC. In this case the observed retrograde mineral paragenesis epidote + paragonite and the observed amphibole and phengite compositions cannot be generated, owing to the lack of water influx during decompression. (2) Homogeneous equilibrium crystallization with water re-saturation (the samples follow the water saturation curves given in Fig. 10). This scenario implies addition of H_2O where the water saturation curve has a negative slope. In this case compositional re-equilibration of amphibole and phengite and thus the compositional zoning, if developed, is unlikely to be step-like. (3) Conservation of the

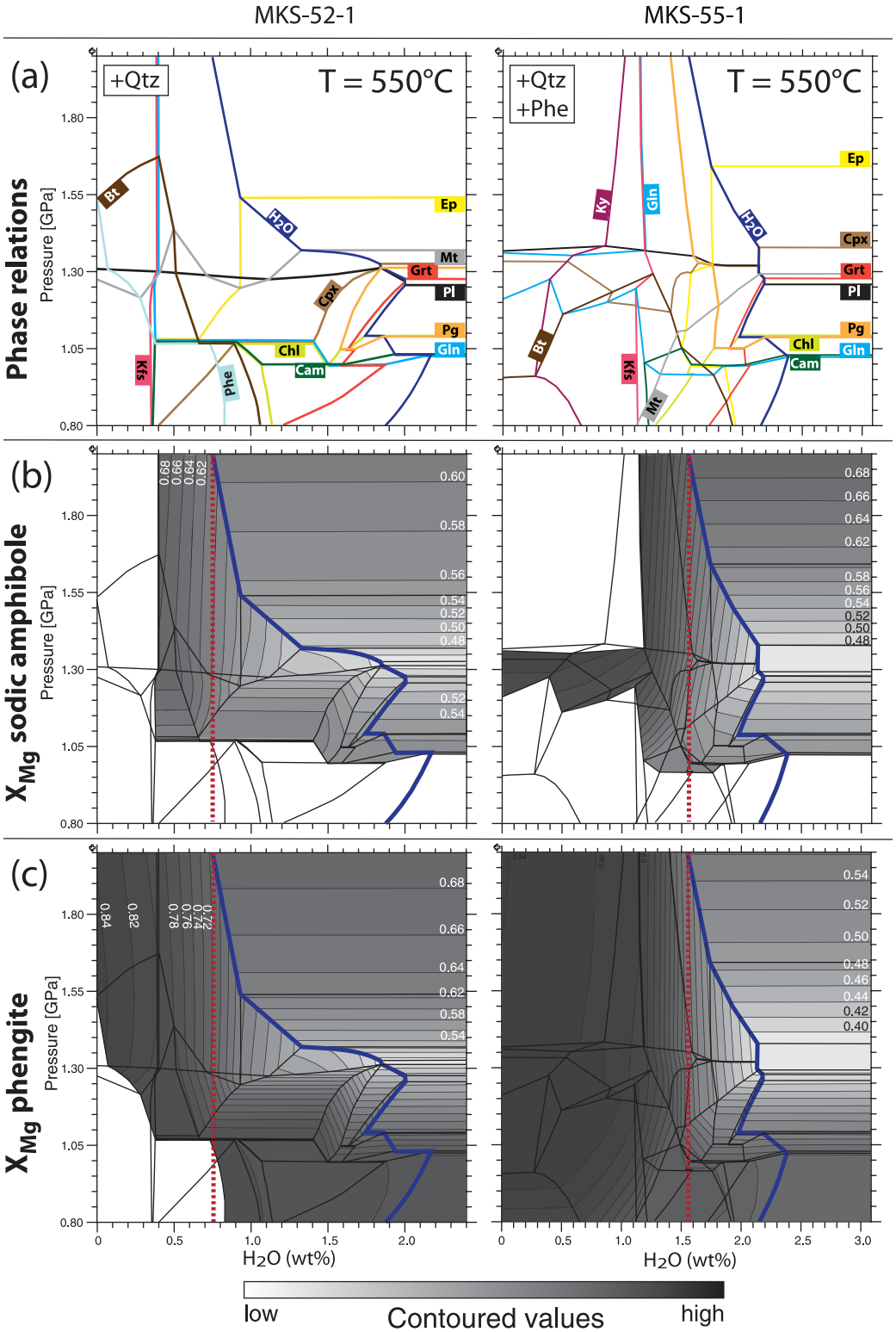

Fig. 10. P-wt % H_2O diagrams calculated for the bulk-rock composition of the samples. (a) Phase relations. The stability field of a certain phase is displayed by the zero mode line and the label of the mineral shown on the 'present' side. (b) Contours for X_{Mg} in amphibole. (c) Contours for X_{Mg} in phengite. Phase fields are as shown in (a). The restricted stability of low-X_{Mg} amphibole and phengite in assemblages close to water saturation should be noted.

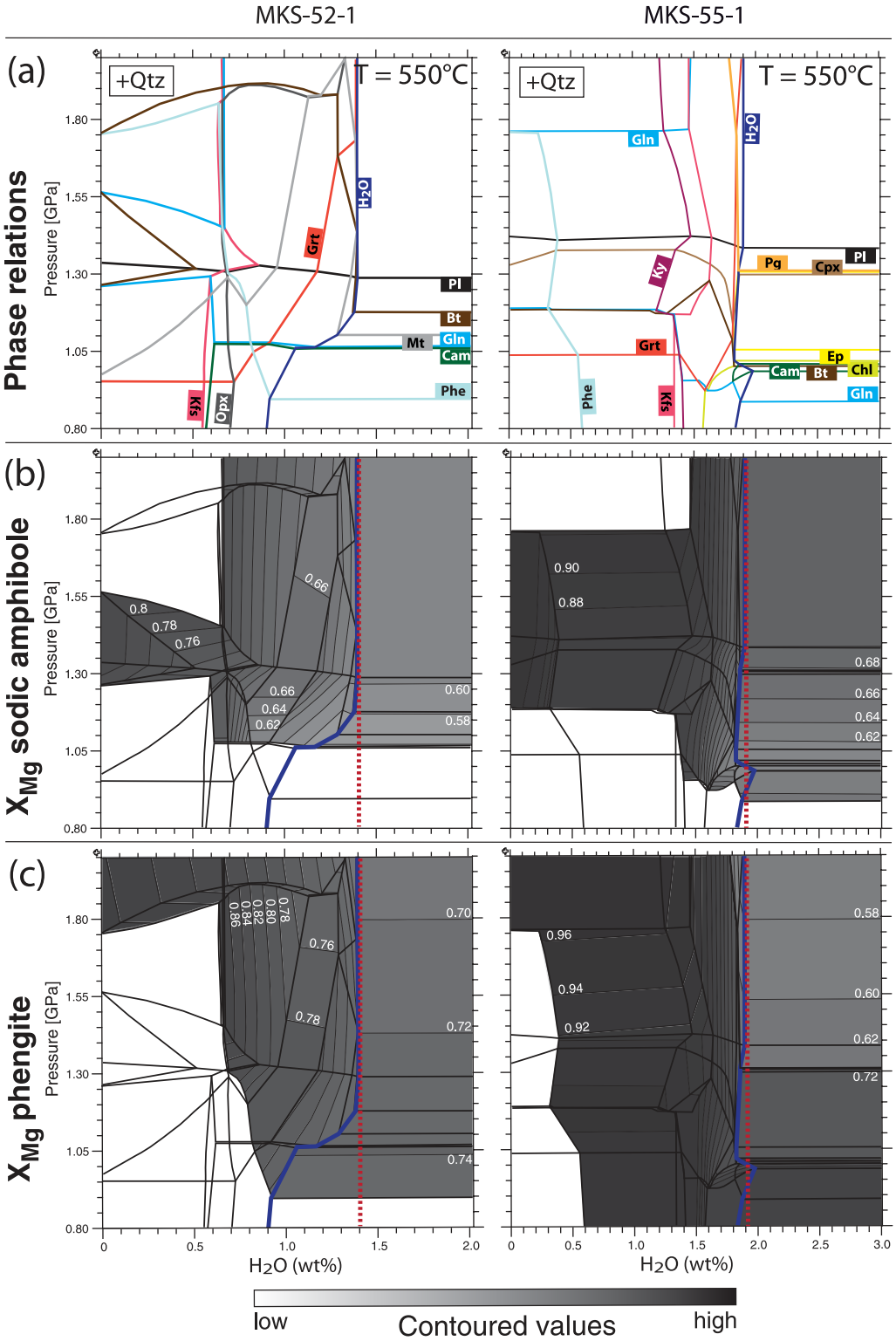

Fig. 11. P-wt % H_2O diagrams calculated for the effective bulk-rock composition of the samples at peak metamorphic conditions. (a) Phase relations, (b) X_{Mg} in amphibole and (c) X_{Mg} in phengite. Without recycling of the fractionated material (garnet) amphibole and phengite do not develop the low X_{Mg} values observed in the natural samples. Details as for Fig. 10.

peak EBC and peak water content without garnet resorption (samples follow the red dotted line in Fig. 11b and c). This last case would indeed maintain water saturation during decompression, but the refractory garnet material hinders the observed compositional re-equilibration of amphibole and phengite, as well as the formation of paragonite in the basic sample.

Forward models for the various scenarios along the retrograde P–T trajectory, which reflect a more detailed evolutionary model for the samples, are shown in subsequent figures. Figure 12 reflects the effect of decreasing pressure during decompression, showing changes in the phase assemblage (a) as well as in phengite (b) and amphibole (c) compositions, assuming homogeneous equilibrium crystallization without water influx; that is, fractionated garnet material is resorbed, but the H_2O contents of the samples remain constant at peak metamorphic values. The most important effect during this scenario is that the initial stages of the exhumation the samples are water-saturated and garnet material is available for the compositional equilibration of the phase assemblage (Fig. 12a). The amount of garnet decreases during decompression and sodic amphibole is formed. Associated with this reaction is a slight decrease in X_{Mg} in phengite and amphibole. As both product phases are hydrous and the amount of water is restricted, the rocks become water undersaturated at around 1·8 GPa (felsic sample) or 1·6 GPa (basic sample). Thus, resorption of garnet and the associated formation of hydrous phases consume the entire available amount of free water. The resulting water undersaturation hinders further compositional re-equilibration of amphibole and phengite during decompression.

The diagrams in Fig. 12 show the importance of water saturation on the mineral assemblage and composition. In Fig. 13 we demonstrate the effect of resorption of previously fractionated garnet material on the re-equilibration of phases and phase compositions. These diagrams (Fig. 13) are calculated for the assumption of a 'rehydrating system'. The samples stay water-saturated during their retrograde evolution, but refractory garnet does not dissolve or react during decompression. Interestingly, the calculated

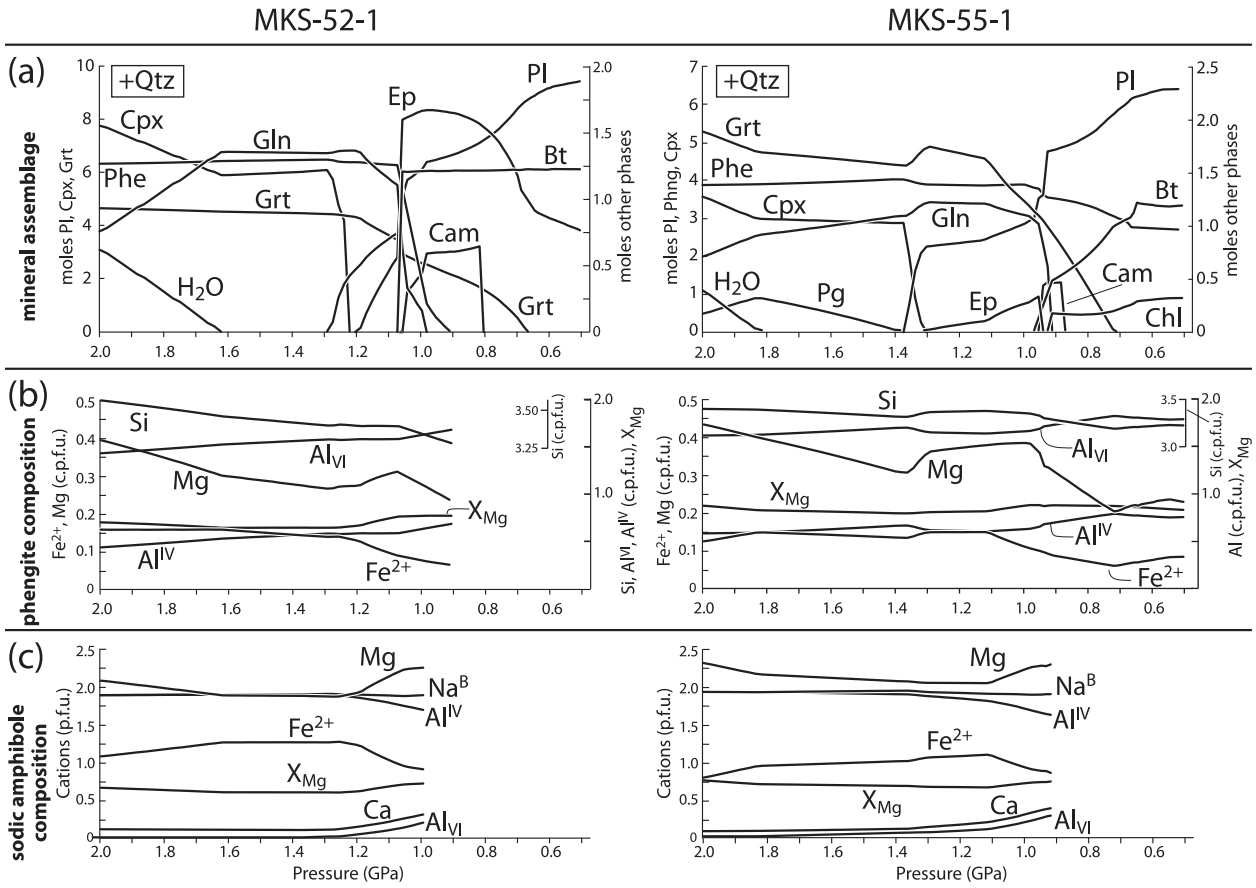

Fig. 12. Phase relations (a), phengite X_{Mg} (b) and amphibole X_{Mg} (c) calculated along the retrograde P–T segment assuming peak EBC and peak water content of the samples but recycling of fractionated garnet material.

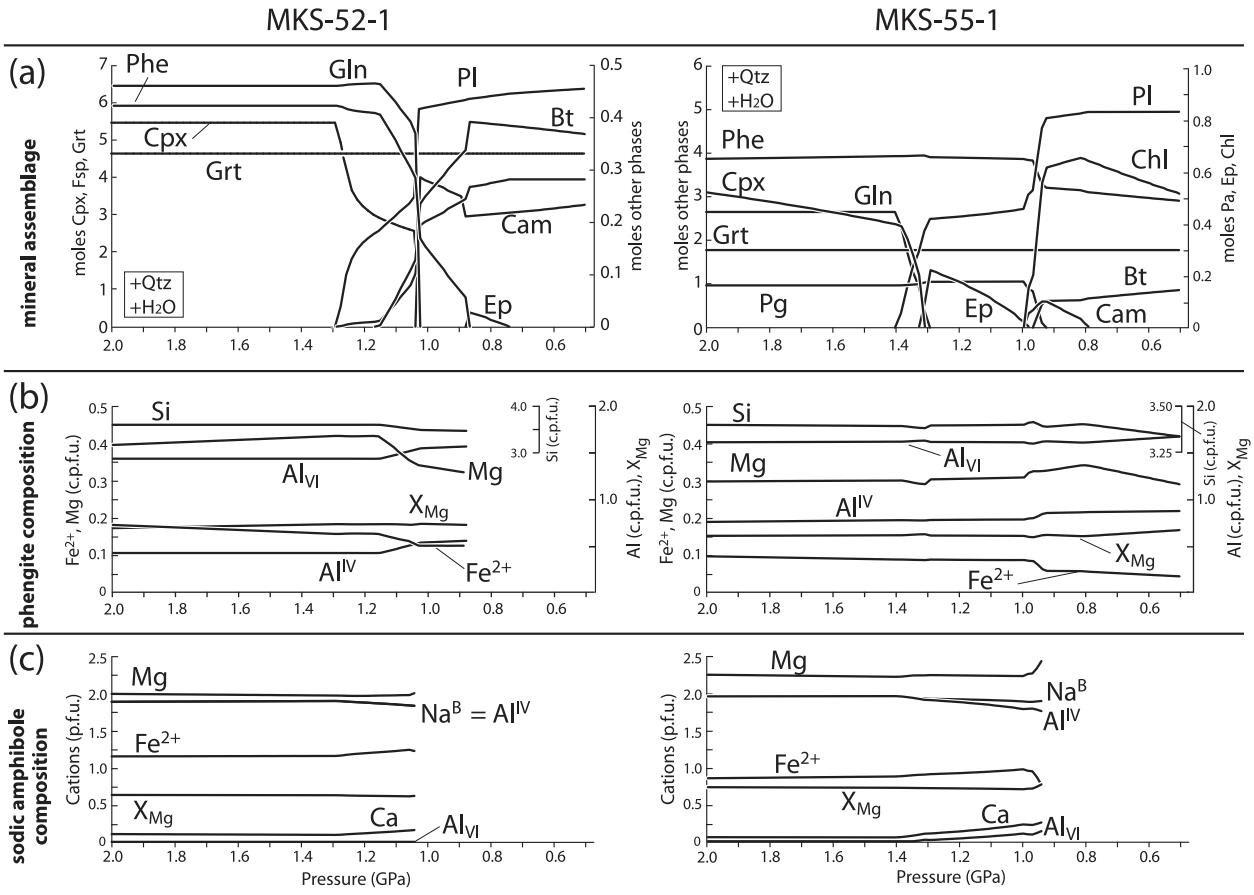

Fig. 13. As for Fig. 12, but without recycling of fractionated garnet material. (See text for discussion.)

amount of newly formed sodic amphibole is very small (a) and the compositional trends of phengite (b) and sodic amphibole (c) are almost constant, which indicates that water influx into the dehydrated and depleted bulk-rock volume without remobilization of the fractionated elements in refractory garnet does not lead to a significant change in the retrograde metamorphic rock evolution. The depleted effective (i.e. reacting) bulk-rock composition, despite being water-present, hinders the compositional re-equilibration of phengite and sodic amphibole.

DISCUSSION

The preservation of multiple stages of retrogression in the mineral assemblages, as well as compositional differences within the mineral grains, allows detailed reconstruction of the retrograde metamorphic evolution of our samples. Comparing the results of the thermodynamic modelling with the observed features in our samples yields important insights into the effect of fluid infiltration on the mineral parageneses and on the major element compositions of the coexisting phases. Further, the pattern of restricted compositional resetting of sodic amphibole (see Faryad & Hoinkes 2004) and phengite (see Dempster, 1992; Giorgis *et al.*, 2000), visible in high-contrast BSE images, allows tracing of the fluid pathways and the regional distribution of fluid influx above a subducted slab.

It should be noted that our thermodynamic calculations were performed in a simplified chemical system (NCKFMASH) with the chemical potential of oxygen (μ_O) being controlled by an ilmenite–magnetite–rutile (IMR) buffer, which constrains the oxidation state of the rocks between the hematite–magnetite (HM) and quartz–fayalite–magnetite (QFM) buffers (see Konrad-Schmolke *et al.*, 2008). Ferric iron is considered in the epidote solid solution as well as in endmember magnetite. It is questionable whether buffering μ_O can adequately describe the oxidation state of a rock (e.g. Diener & Powell, 2010); however, in the absence of a complete set of thermodynamic data for ferric iron-bearing solid solution phases and under consideration of an open-system behavior of our samples, buffering μ_O seems a reasonable compromise. Furthermore, ignoring ferric iron in omphacite and amphibole solid solutions might underestimate the extent of stability of both phases. Whereas ferric iron in amphibole

is low in our samples (usually <10% Fe_{tot}), it is present in considerable amounts in omphacite in the felsic sample (Fig. 4). However, calculations utilizing the latest thermodynamic data for ferric iron endmembers in omphacite (Green *et al.*, 2007) and amphibole (Diener *et al.*, 2007) solid solutions show that omphacite might be stable in all plagioclase-absent assemblages (i.e. above 1·0–1·4 GPa, depending on temperature), but, similar to our simplified calculations, giving way to an assemblage with increasing epidote, sodic amphibole and plagioclase during breakdown (see Electronic Supplementary Data). As the focus of this work is on the effect of water influx on changes in the mineral assemblage, rather than on specifying the exact metamorphic P–T conditions of our samples, we assume that a slightly underestimated stability of omphacite has only minor effect on our conclusions.

Water re-saturation and amount of infiltrated fluid

At peak metamorphic conditions the stable mineral paragenesis of the samples was garnet + omphacite + glaucophane-rich sodic amphibole + phengite + quartz ± epidote ± paragonite. This assemblage is only partly preserved in the samples. The calculated water content of these assemblages at peak conditions was around 1·5 wt % in the felsic samples and between 0·6 and 1·3 wt % in the basic samples (Fig. 6). Most interesting is the partial re-equilibration of our samples during exhumation. The observed modal relations in the overprinted areas (i.e. the formation of hydrous phases such as phengite and epidote after omphacite, as well as the characteristic often step-like compositional trends in phengite and sodic amphibole) are clear evidence for one or more discrete fluid influx stages during decompression. As shown in the P–XH_2O diagrams in Fig. 10, the observed compositions of the overprinted areas of sodic amphibole ($X_{Mg} = 0{\cdot}5$) and phengite ($X_{Mg} = 0{\cdot}6$) are highly indicative of the coexistence of these phases in specific stability fields where both phases form a characteristic X_{Mg} minimum. The observed compositions of phengite and sodic amphibole are calculated to be stable at (near-) water-saturated conditions between 1·4 and 1·2 GPa only. The diagrams in Fig. 7, which display the calculated compositional evolution of phengite and sodic amphibole at water-saturated conditions along the proposed P–T trajectory, also show this distinct X_{Mg} minimum. However, the modelled, relatively smooth compositional trends in phengite and sodic amphibole are in contrast to the observed trends, which show dramatic, step-like core-to-rim transitions from high to low X_{Mg} values (Figs 3 and 4). Assuming continuous metamorphic evolution and homogeneous equilibrium crystallization, both phases would exhibit either no or only smooth compositional gradients, even in the case of sluggish diffusional relaxation and the development of compositional growth zonation. Thus, it is much more likely that the observed compositional trends are the result of discontinuous compositional equilibration. Based on the thermodynamic calculations, such a discontinuity can be best explained by an initial decompression without water addition, which led only to moderate compositional changes in amphibole and phengite (e.g. Fig. 11), followed by one or more discrete fluid influx events between 1·4 and 1·2 GPa, which allowed rapid water re-saturation and (partial) compositional equilibration of the mineral assemblage. It is likely that during initial decompression and cooling the rocks became water undersaturated owing to the limited external water influx. This effect is evident from the preservation of the Mg-rich compositions of phengite and sodic amphibole. Limited water availability additionally hindered the compositional re-equilibration, owing to sluggish reaction kinetics and slow element transport (e.g. Rubie, 1986; Stünitz, 1989).

Some constraints on the amount of fluid necessary to re-establish water saturation in the overprinted areas of the samples can be estimated. It is important to note that all thermodynamic calculations in this study are based on normalization of the coexisting phases to represent 100% of the reacting rock volume. Thus, quantification of the absolute amounts of fluids and solids must take into account that only a fraction of the entire rock volume has reacted during the fluid influx. This is critical if we quantify the absolute amount of infiltrated fluid or a fluid–rock ratio. It is evident that the amount of the infiltrated fluid led to water saturation only in the overprinted rims, but was not large enough—or the reaction kinetics were too sluggish—to re-equilibrate the entire rock volume.

Nevertheless, rough estimates can be made for the amount of the infiltrating fluid during metamorphism. It can be seen in thin section as well as in BSE images that (1) almost the entire amount of omphacite in our samples has been consumed by retrograde reactions, (2) estimating from the BSE images shows that about 10% of mica and 20% of the sodic amphibole by volume are overprinted and recrystallized, and (3) the amount of the greenschist-facies overprint is clearly below 5% of the entire rock volume. A conservative estimate of the reacted rock volume during the blueschist-facies fluid influx is around 20% of the entire rock volume. The isothermal P–XH_2O diagrams in Fig. 10, as well as the forward model results shown in Fig. 7, indicate that about 1·2 and 0·6 wt % water must be added in sample MKS-52-1 and MKS-55-1 respectively, to re-saturate the entire rock with respect to water, to yield the stability of the observed assemblage and to produce the observed Mg trends in mica and sodic amphibole (see Figs 4 and 6). Assuming about 20% of the entire rock to be re-equilibrated during fluid influx, the amount of the percolating fluid in these samples must be around 0·2 and 0·1 wt % in sample MKS-52-1 and MKS-55-1 respectively, to ensure water re-saturation

in the affected areas. From the results shown in Fig. 10, this fluid influx occurred between 1·4 and 1·2 GPa. However, these values do not give a clear idea about the time-integrated fluid flux, as they do not involve the length-scale of the fluid migration, estimation of which is difficult because of the large-scale structures in the SLZ (e.g. Gosso *et al.*, 1979; Zucali *et al.*, 2002; Babist *et al.*, 2006). A minimum length-scale is given by the vertical thickness of overprinted samples in an observable, structurally coherent profile, which is of the order of 2 km. This would correspond to a time-integrated fluid flux of about $15\,m^3\,m^{-2}$. A less conservative estimate would assume that the length-scale of fluid migration is constrained by the present vertical extent of the SLZ, which can only be estimated from seismic profiles (e.g. Schmid & Kissling, 2000) and is of the order of 10 km. This vertical column would require a time-integrated fluid flux of $75\,m^3\,m^{-2}$ to produce the observed re-equilibration textures. Both estimates yield fairly modest fluid fluxes through the moderately deformed internal SLZ, although the intensity of fluid migration and fluid–rock interaction might change depending on the mode of fluid transport, as discussed further below.

Regional fluid flux and fluid pathways

Fluid flux in metamorphic rocks might be related to brittle deformation (e.g. along veins; Cartwright & Buick, 2000; Oliver & Bons, 2001), to ductile deformation (e.g. along shear zones; Austrheim, 1987; Bebout & Barton, 1993) or be pervasive via an interconnected fluid film along grain boundaries and other microstructures (de Meer *et al.*, 2005; Keller *et al.*, 2006). Deformation-induced fluid flux is often associated with limited fluid–rock interaction in undeformed areas and allows large quantities of fluid to migrate through a rock volume without significant compositional effects on either fluid or wall-rock (e.g. Austrheim, 1987; Barnicoat & Cartwright, 1995). In contrast, large-scale pervasive fluid flux along grain boundaries, as in our samples, allows intense fluid–rock interaction with strong chemical and physical effects on the fluid and the wall-rocks. The consequences of reactive fluid flux above a subducted slab have been demonstrated by trace element and isotopic studies of mélange zones and exhumed high-pressure sequences (e.g. Sorensen *et al.*, 1997; Marschall *et al.*, 2006; Penniston-Dorland *et al.*, 2010), which show that pervasive fluid fluxes heavily modify the elemental and isotopic composition of the wall-rocks and the fluid. Because compositional re-equilibration of our samples is incomplete and newly formed, as well as re-equilibrated, phases can be easily distinguished in high-contrast BSE images, our samples are excellently suited to study regional-scale fluid infiltration and fluid–rock interaction, which is important for the general understanding of fluid-driven mass transfer in the Earth's crust and, in particular, in subduction zones.

There are four types of fluid-assisted re-equilibration textures visible in our samples: (1) brittle fracturing within amphiboles with subsequent precipitation of new equilibrated amphibole material (Fig. 3a); (2) precipitation of new phengite and amphibole material along grain boundaries (Fig. 3c, d and h); (3) migration of reaction fronts from grain boundaries concentrically into undeformed grains (Fig. 3d, e and f); (4) re-equilibration by volume diffusion that produces a continuous compositional change perpendicular to the grain boundaries (arrows in Fig. 3c, d and h). Many of the re-equilibrated areas in our samples are of type (2) and (3), both of which occur along almost all grain boundaries (Fig. 3c, d, e and f). The observation that this kind of overprinting occurs along almost the entire grain boundary network, together with our thermodynamic calculations, which show that fluid influx is necessary to produce the newly formed rim compositions and overgrowths, suggests the presence of an interconnected network, probably wetted by a free fluid phase, along the grain boundaries (see Rubie, 1986). Such a regional-scale, open-system pervasive and reactive fluid flux (e.g. Ferry, 1987, 1992) allowed effective elemental exchange and compositional re-equilibration of fluids and wall-rocks.

Many experimental studies and natural examples (e.g. Holness, 1993; Hippertt, 1994; Mancktelow & Pennacchioni, 2004) suggest the existence of non-interconnected porosity along grain boundaries in undeformed rocks that might become interconnected during deformation and changing confining pressure (e.g. Holness, 1993; Fusseis *et al.*, 2009). Recent work also suggests the existence of a continuous fluid film of several nanometres width along grain boundaries under static metamorphic conditions (e.g. de Meer *et al.*, 2005; Keller *et al.*, 2006). Nakamura & Watson (2001) experimentally showed that as a result of dissolution–precipitation processes, wetting fluids, such as aqueous solutions, can migrate in the form of advancing high-porosity zones in quartzites. These findings are similar to our observation of newly precipitated sodic amphibole along existing grain boundaries (Fig. 3h) and the occurrence of re-equilibration fronts that migrate into older grains (Fig. 3f).

The development of micro-porosity is, however, difficult to explain in rocks undergoing mineral reactions with a positive volume change. In our samples, the rock volume owing to retrograde mineral reactions increases from eclogite- to blueschist-facies conditions by 5% in the felsic and 8% in the basic sample. Up to greenschist-facies conditions the volume increases by 10 and 17% in the felsic and basic sample, respectively (Fig. 7d). The fluid influx event and the associated mineral reactions alone are associated with a volume increase of about 1·8%. Thus dilatancy owing to negative volume changes seems to be unlikely for the generation of any permeability; however,

recent studies (e.g. Jamtveit *et al.*, 2008) provide evidence for the development of an extensive network of brittle fractures and/or sub-grain boundaries in initially low-permeability rocks by mineral reactions that are associated with a volume increase. It is notable that the microfractures and/or interconnected sub-grain boundaries shown in Fig. 3h are very similar to the textures developed in the models of Jamtveit *et al.* (2008), as well as in several other experiments (e.g. Putnis, 2002; Milke & Wirth, 2003), and seem to be common in naturally occurring, high-pressure/low-temperature rocks (e.g. Konrad-Schmolke *et al.*, 2007). However, the existence of an interconnected fluid film along grain boundaries in our samples is contrary to observations in many retrograde high-pressure rocks from within the subducted slab, in which fluid migration is often connected to brittle fracturing or restricted to shear zones (e.g. Austrheim, 1987; Cartwright & Buick, 2000; Franz *et al.*, 2001; John & Schenk, 2003). This is, of course, important for containing the extent of the fluid–rock interaction in our samples, but also for the initiation of solution and re-precipitation processes (e.g. de Meer *et al.*, 2005) that might explain the observed intra-grain step-like re-equilibration features in our samples.

Open-system pervasive fluid flow is important at mid- and upper-crustal levels and in hydrothermal systems associated with regional metamorphism (e.g. Ferry, 1987, 1988, 1992; Cartwright *et al.*, 1995; St-Onge & Lucas, 1995); similar examples are also reported for subduction-zone settings, such as the mantle wedge (e.g. Peacock, 1987; Kostenko *et al.*, 2002) or the slab–mantle interface (e.g. Bebout & Barton, 1993). In the hanging wall of a subducted slab, where strong, thermally induced gradients in hydraulic head exist and where buoyancy-driven upward migration of fluids liberated by dehydration reactions in the downgoing slab is a likely process, the prerequisites for pervasive fluid flux along grain boundaries are generally met (e.g. Oliver, 1996). Thus, pervasive fluid flow might be a common process, especially in larger, weakly deformed coherent blocks that undergo exhumation at the top of the subducted slab. Thus, interpretation of the trace element and isotopic composition of subduction-related volcanic rocks must consider the potential for significant compositional modification of primary devolatilization fluids at the slab–mantle interface.

Generally, there is likely to be a dramatic change in the overall fluid flow mechanism from within the subducted slab, across the slab–mantle interface into the hanging wall mantle wedge (Fig. 14). In the downgoing subducted slab most prograde mineral reactions are associated with a negative volume change, which allows the formation of open fractures that channelize fluid flow (e.g. John & Schenk, 2003; Zack & John, 2007). In contrast, as demonstrated by our examples, rocks in the hanging wall of the subducted slab are often affected by retrograde and/or re-hydration reactions, owing to decompression or fluid infiltration, or both. Such reactions are often associated with a positive volume change (Fig. 7d) and thus dilatancy, and the possibility of vein formation is limited. In this setting, fluid migration is controlled either by viscous deformation and channelized in ductile shear zones, or by the development of microfractures as a response to the internal strain distributed among and around mineral grains. Several workers (e.g. Sorensen, 1988; Sorensen *et al.*, 1997; Breeding *et al.*, 2003) have shown inhomogeneous and incomplete retrogression of high-pressure rocks in mélange blocks that are interpreted to represent parts of the slab–mantle interface. Fluid flux in these examples is concentrated around low-permeability regions ranging from centimetre- to decametre-sized undeformed blocks of eclogite material that is surrounded by a highly deformed and highly permeable matrix (e.g. Ague, 2007).

Our samples represent a similar situation, although on a different scale. During exhumation of the Mombarone Unit strain was partitioned between large-scale blueschist-facies shear zones bounding the Mombarone Unit and weakly deformed rocks in the internal parts (Babist *et al.*, 2006). Mylonitic rocks are well equilibrated under retrograde blueschist-facies conditions (Stünitz, 1989; Babist *et al.*, 2006), whereas our samples from weakly deformed, internal, initially less permeable regions of the Mombarone Unit reflect only moderate fluid influx, although associated with an intense retrograde overprint in the affected areas. Although fluids might be carried away rapidly, and without strong interaction, from the subducting slab (e.g. Zack & John, 2007), it is evident that intense fluid–rock interaction occurs on top of the slab, which significantly modifies the trace element composition of the subduction-related fluid in the highly reactive slab–mantle transition zone.

Above the slab–mantle transition zone the mode of fluid migration, and therefore the extent of fluid–rock interaction in the mantle wedge, is crucial for the understanding of mantle hydration, major- and trace-element transfer, melt generation and migration, as well as for the boundary conditions of numerical thermal models of subduction zones (e.g. Iwamori, 1998; Arcay *et al.*, 2005). Pervasive fluid flux seems to be the common mechanism for fluid- and also melt migration in the mantle wedge (e.g. Lundstrom, 2000; Kostenko *et al.*, 2002), although some examples also exist of a channelized fluid influx into the mantle wedge (e.g. Bodinier *et al.*, 1990). Based on the interpretation of seismic data (Bostock *et al.*, 2002; Xia *et al.*, 2008) the hydration of the mantle wedge above subducted slabs seems to be inhomogeneous, which provides further evidence for inhomogeneous fluid fluxes, but, unfortunately, provides few constraints on the mode of fluid migration on a larger scale.

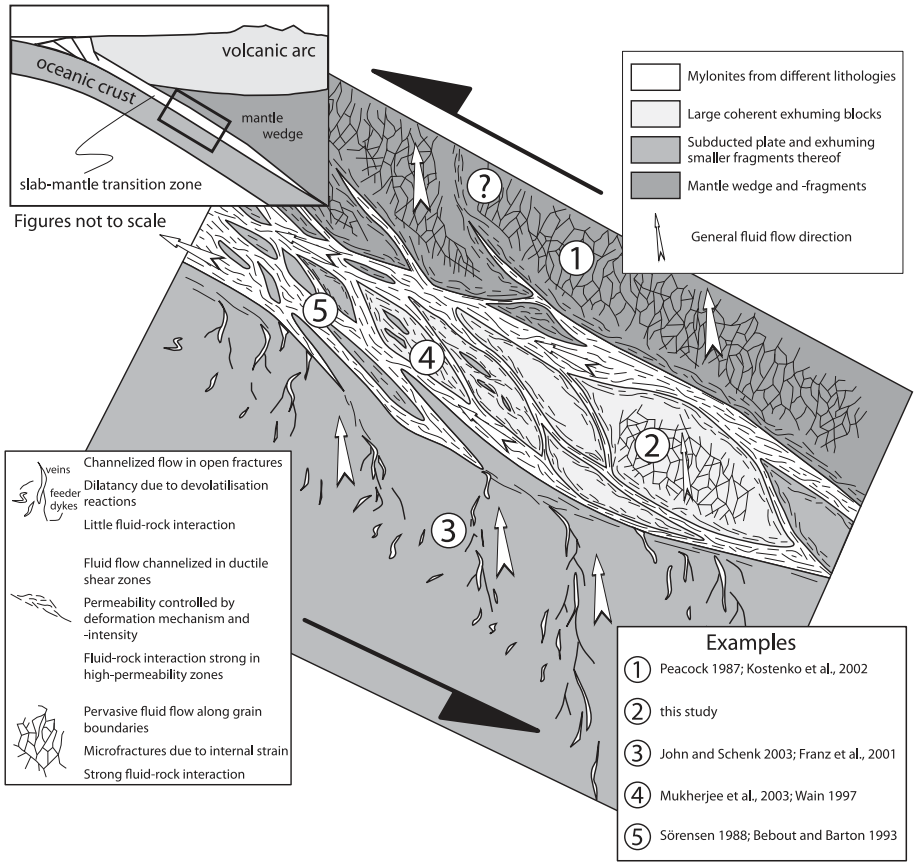

Fig. 14. Schematic illustration of fluid migration pathways in a subduction zone. Within the subducted slab fluid flux is channelized and fluid–rock interaction limited owing to the development of veins by prograde mineral reactions with negative volume change. In the slab–mantle transition zone fluid flux is controlled by the extent of viscous deformation and is mostly parallel to the slab–mantle interface. Pervasive fluid flux is possible owing to retrograde mineral reactions with positive volume change. In the mantle wedge fluid flux is pervasive or might regionally be controlled by viscous deformation. For examples see Bebout and Barton, 1993; Franz *et al.*, 2001; John and Schenk, 2003; Kostenko *et al.*, 2002; Mukherjee *et al.*, 2003; Peacock, 1987; Sörensen, 1988; Wain, 1997.

Rate-controlling processes

Reaction-controlled element availability and the limited compositional resetting of phengite and sodic amphibole during fluid influx is interesting with respect to the rate-controlling processes of rock retrogression and of fluid–rock interaction. Figure 13 shows the calculated phase assemblages and amphibole compositions of the effective bulk-rock composition at peak metamorphic conditions for the two selected samples along the specified P–T trajectory. The calculations assume that fractionated garnet does not back-react and thus that all elements incorporated into the garnet interiors are isolated from the reacting bulk-rock volume, implying garnet-absent conditions during decompression, as the material in the interiors of the porphyroblasts is not available for thermodynamic equilibration. A comparison of the results shown in Fig. 12 indicates that even with re-saturation of the rocks with respect to water there is no thermodynamically controlled Fe enrichment predicted in phengite and amphibole. In contrast, as shown in Fig. 7, recycling of garnet material is the controlling factor for the stabilization of iron-rich areas in phengite and amphibole. Thus, garnet, the kinetically most retentive phase in our samples, controls the extent of recrystallization and re-equilibration. In other words, resorption of garnet material from the porphyroblasts (i.e. recycling of garnet material into the EBC) is necessary to allow compositional re-equilibration of amphibole and phengite and to produce the observed X_{Mg} decrease in the natural samples. In turn, the spatial extent of phengite and amphibole overprinting can provide information about the transport distances and the properties of the recycled garnet material (e.g. iron content) in the samples. Although Mn back-diffusion and newly formed Mn-rich overgrowth zones on garnets from our samples (Fig. 4h) are clear indications of garnet resorption during fluid infiltration, textural relations do not allow

a spatial correlation of garnet resorption sites and the intensity of X_{Mg} re-equilibration in phengite and sodic amphibole.

The above observation suggests that garnet porphyroblasts have multiple significance in high-pressure rocks. They might contrain the physical behaviour of the rock (e.g. Groome *et al.*, 2006), they might control element recycling into the mantle (e.g. Konrad-Schmolke *et al.*, 2008*a*) and they might further control the extent of preservation of high-pressure assemblages in exhumed rocks because of their sluggish reaction rates, which in turn significantly influences the coexisting phases.

Major element transport in the fluid

The compositional profiles and element maps of phengite and amphibole (Figs 4 and 5b and c) show a predominant Fe–Mg exchange towards higher Fe contents in the overprinted areas of both minerals. Ca is also slightly enriched in the overprinted areas of sodic amphibole. As the overprinting effect is fluid-controlled, all three elements must be sufficiently present in the transport agent to allow re-equilibration of the affected areas. The length-scale of element transport is at least at the thin-section scale, because there is no preferential overprinting of phengite and amphibole around Fe- and Ca-rich minerals such as omphacite and garnet. There is still insufficient knowledge about the properties of subduction-related fluids (Manning, 2004), and the solubility and transport of different elements in such fluids is difficult to constrain experimentally. There have been several studies on fluid inclusions from high-pressure veins in exhumed eclogitic rocks, as well as data from fore-arc serpentinites (e.g. Becker *et al.*, 1999; Fryer *et al.*, 1999; Franz *et al.*, 2001; Gao & Klemd, 2001). Most of these studies indicated a significant mobilization of major elements, such as Si, Al, Na, Ca and Mg; however, none of these studies concentrated on the amount of dissolved iron, which is clearly mobile in our samples. The formation of Fe-rich minerals, such as omphacite and garnet, within high-pressure veins suggests significant transport of Fe in subduction zone fluids (Philippot & Selverstone, 1991; Franz *et al.*, 2001). Furthermore, there is clearly addition of potassium during fluid influx, which is evident from the formation of phengite-rich pseudomorphs after omphacite (see Rubie, 1986). Interestingly, newly formed phengite does not precipitate along the edges of existing grains, which would be the favoured site of precipitation considering the surface energy constraints, but instead forms preferentially at omphacite reaction sites. We interpret the replacement of omphacite by phengite as a result of the limited availability of Al in the percolating fluid. It is likely that the K/Al ratio in the fluid is too large to allow phengite precipitation along existing phengite grain boundaries. Only at those sites where Al is available as a result of retrograde net-transfer reactions, such as omphacite breakdown, can new phengite form. This observation suggests limited mobility of Al in our samples; however, abundant K needs to be present in the fluid (e.g. Philippot & Selverstone, 1991). Rubie (1986) attributed the observed K-metasomatism to a large fluid/rock ratio that might partially be present in these rocks. It is obvious that water saturation must have prevailed during this non-isochemical reaction as hydrous K-bearing phases formed from omphacite, which does not contain K or even inclusions of phengite prior to the fluid influx (see Rubie, 1986). However, the presence of chlorine in the fluid, which is indicated by the higher Cl contents in the overprinted phengite rims (Fig. 4g), certainly plays a major role regarding the relatively high solubility and transport of major elements in our samples (e.g. Manning, 2004).

CONCLUSIONS

The Western Alpine Sesia Zone is a segment of continentally derived high-pressure rocks that were exhumed in the hanging wall of a subducted oceanic plate. Fluid infiltration into the previously dehydrated rocks led to partial retrogression during exhumation. Weakly deformed samples from the internal part of the SLZ well preserve relict eclogite-facies mineral assemblages. Limited fluid influx into relatively dry, high-pressure rocks led to complex and characteristic compositional zonation patterns in phengite and sodic amphibole that are best visible in high-contrast BSE images. The effect of the fluid influx is reflected in a complex network of modified amphibole and phengite that appears brighter in BSE images and has sharp boundaries with the unaffected cores. Differences between overprinted and shielded areas in both minerals are mainly in the X_{Mg} value, with lower X_{Mg} in the overprinted rims. The concentrations of fluid-mobile trace elements, such as Ba and Sr, increase and decrease from core to rim, respectively. Furthermore, fluid infiltration caused the formation of unusual phengite–epidote–albitic plagioclase pseudomorphs after omphacite. A comparison of the observed textural and compositional changes in our samples with thermodynamic models yields insight into the amount and major element composition of the infiltrated fluid. Only *c.* 0·1–0·5 wt % fluid relative to the entire rock was added during exhumation. Furthermore, the observation of the fluid-induced retrogression features over map-scale distances indicates open-system, pervasive fluid infiltration and intense fluid–rock interaction at blueschist-facies conditions above a subducted slab. Fluid infiltration caused K-metasomatism and allowed intense Fe–Mg exchange among coexisting minerals, but did not cause mobilization of large amounts of Al. We propose that these samples are extremely well suited for the investigation of fluid-triggered high-pressure processes in a subduction zone from (sub-)grain to regional scale, and that the

compositional resetting of sodic amphibole and phengite can be used as an excellent tracer of the fluid–rock interaction.

ACKNOWLEDGEMENTS

We thank Horst Marschall (Woods Hole) and Michel Marks (Tübingen) for inspiring discussions about fluid migration. James Scott and Christina Günter are thanked for assistance with the electron microprobe analyses. We additionally thank Jörg Herrman for thoughtful editorial handling, as well as Jay Ague, Daniele Castelli and Peter Tropper for thorough, critical and constructive reviews.

SUPPLEMENTARY DATA

Supplementary data for this paper are available at *Journal of Petrology* online.

REFERENCES

Ague, J. J. (2007). Models of permeability contrasts in subduction zone mélange: Implications for gradients in fluid fluxes, Syros and Tinos islands, Greece. *Chemical Geology* **239(3–4)**, 217–227.

Arcay, D., Tric, E. & Doin, M.-P. (2005). Numerical simulation of subduction zones. Effect of slab dehydration on the mantle wedge dynamics. *Physics of the Earth and Planetary Interiors* **149**, 133–153.

Austrheim, H. (1987). Eclogitization of lower crustal granulites by fluid migration through shear zones. *Earth and Planetary Science Letters* **81(2–3)**, 221–232.

Babist, J., Handy, M. R., Konrad-Schmolke, M. & Hammerschmidt, K. (2006). Precollisional, multistage exhumation of subducted continental crust: The Sesia Zone, Western Alps. *Tectonics* **25(6)**, TC6008.

Barnicoat, A. C. & Cartwright, I. (1995). Focused fluid flow during subduction: Oxygen isotope data from high-pressure ophiolites in the Western Alps. *Earth and Planetary Science Letters* **132**, 53–61.

Bebout, G. E. & Barton, M. D. (1993). Metasomatism during subduction: Products and possible paths in the Catalina schist, California. *Chemical Geology* **108(1–4)**, 61–92.

Bebout, G. E., Ryan, J. G., Leeman, W. P. & Bebout, A. E. (1999). Fractionation of trace elements by subduction-zone metamorphism—effect of convergent-margin thermal evolution. *Earth and Planetary Science Letters* **171(1)**, 63–81.

Bebout, G. E. & Barton, M. D. (2002). Tectonic and metasomatic mixing in a high-*T*, subduction-zone mélange—insights into the geochemical evolution of the slab–mantle interface. *Chemical Geology* **187(1–2)**, 79–106.

Becker, H., Jochum, K. P. & Carlson, R. W. (1999). Constraints from high-pressure veins in eclogites on the composition of hydrous fluids in subduction zones. *Chemical Geology* **160(4)**, 291–308.

Bodinier, J. L., Vasseur, G., Vernières, J., Dupuy, C. & Fabriès, J. (1990). Mechanisms of mantle metasomatism: Geochemical evidence from the Lherz orogenic peridotite. *Journal of Petrology* **31(3)**, 597–628.

Bostock, M. G., Hyndman, R. D., Rondenay, S. & Peacock, S. M. (2002). An inverted continental Moho and serpentinization of the forearc mantle. *Nature* **417**, 536–538.

Bouvier, A.-S., Metrich, N. & Deloule, E. (2008). Slab-derived fluids in the magma sources of st. Vincent (Lesser Antilles arc): Volatile and light element imprints. *Journal of Petrology* **49(8)**, 1427–1448.

Breeding, C. M., Ague, J. J., Bröcker, M. & Bolton, E. W. (2003). Blueschist preservation in a retrograded, high-pressure, low-temperature metamorphic terrane, Tinos, Greece: Implications for fluid flow paths in subduction zones. *Geochemistry, Geophysics, Geosystems* **4(1)**, 9002.

Carraro, F., Dal Piaz, G. V. & Sacchi, R. (1970). Serie di Valpelline e II Zona Diorito–Kinzigitica sono i relitti di un ricoprimento proveniente dalla Zona Ivrea–Verbano. *Memorie della Societa Geologica Italiana* **9**, 197–224.

Cartwright, I., Vry, J. & Sandiford, M. (1995). Changes in stable isotope ratios of metapelites and marbles during regional metamorphism, Mount Lofty Ranges, South Australia: Implications for crustal scale fluid flow. *Contributions to Mineralogy and Petrology* **120(3)**, 292–310.

Cartwright, I. & Buick, I. S. (2000). Fluid generation, vein formation and the degree of fluid–rock interaction during decompression of high-pressure terranes: The Schistes Lustrés, Alpine Corsica, France. *Journal of Metamorphic Geology* **18(6)**, 607–624.

Castelli, D. (1991). Eclogitic metamorphism in carbonate rocks; the example of impure marbles from the Sesia–Lanzo Zone, Italian Western Alps. *Journal of Metamorphic Geology* **9(1)**, 61–77.

Compagnoni, R., Dal Piaz, G. V., Hunziker, J. C., Gosso, G., Lombardo, B. & Williams, P. F. (1977). The Sesia–Lanzo Zone, a slice of continental crust with Alpine high pressure–low temperature assemblages in the Western Italian Alps. *Rendiconti della Societa Italiana di Mineralogia e Petrologia* **33(2)**, 335–374.

Dal Piaz, G. V., Gosso, G. & Martinotti, G. (1971). La II Zona Diorito–Kinzigitica tra la Valle Sesia e la Valle d'Ayas (Alpi Occidentali). *Memorie della Societa Geologica Italiana* **11**, 433–460.

Dal Piaz, G. V., Hunziker, J. C. & Martinotti, G. (1972). La Zona Sesia–Lanzo e l'evoluzione tettonico-metamorfica delle Alpi Nordoccidentali interne. *Memorie della Societa Geologica Italiana* **11**, 433–466.

de Capitani, C. & Brown, T. H. (1987). The computation of chemical equilibrium in complex systems containing non-ideal solutions. *Geochimica et Cosmochimica Acta* **51(10)**, 2639–2652.

de Meer, S., Spiers, C. J. & Nakashima, S. (2005). Structure and diffusive properties of fluid-filled grain boundaries: An *in-situ* study using infrared (micro) spectroscopy. *Earth and Planetary Science Letters* **232(3–4)**, 403–414.

Dempster, T. J. (1992). Zoning and recrystallization of phengitic micas: Implications for metamorphic equilibration. *Contributions to Mineralogy and Petrology* **109(4)**, 526–537.

Diener, J. F. A., Powell, R., White, R. W. & Holland, T. J. B. (2007). A new thermodynamic model for clino- and orthoamphibole in the system Na_2O–CaO–FeO–MgO–Al_2O_3–SiO_2–H_2O–O. *Journal of Metamorphic Geology* **25**, 631–656.

Diener, J. F. A. & Powell, R. (2010). Influence of ferric iron on the stability of mineral assemblages. *Journal of Metamorphic Geology* **28**, 599–613.

Duchêne, S., Blichert-Toft, J., Luais, B., Télouk, P., Lardeaux, J. M. & Albarede, F. (1997). The Lu–Hf dating of garnets and the ages of the Alpine high-pressure metamorphism. *Nature* **387**, 586–589.

Escher, A. & Beaumont, C. (1997). Formation, burial and exhumation of basement nappes at crustal scale: A geometric model based on the Western Swiss–Italian Alps. *Journal of Structural Geology* **19(7)**, 955–974.

Faryad, S. W. & Hoinkes, G. (2004). Complex growth textures in a polymetamorphic metabasite from the Kraubath Massif (Eastern Alps). *Journal of Petrology* **45(7)**, 1441–1451.

Ferraris, C. & Compagnoni, R. (2003). Metamorphic evolution and significance of a serpentinized peridotite slice within the Eclogitic

Micaschist Complex of the Sesia-zone (Western Alps–Italy). *Schweizerische Mineralogische und Petrographische Mitteilungen* **83(1)**, 3–13.

Ferry, J. M. (1987). Metamorphic hydrology at 13-km depth and 400–550°C. *American Mineralogist* **72(1–2)**, 39–58.

Ferry, J. M. (1988). Infiltration-driven metamorphism in northern New England, USA. *Journal of Petrology* **29(6)**, 1121–1159.

Ferry, J. M. (1992). Regional metamorphism of the Waits River Formation, Eastern Vermont: Delineation of a new type of giant metamorphic hydrothermal system. *Journal of Petrology* **33(1)**, 45–94.

Franz, L., Romer, R. L., Klemd, R., Schmid, R., Oberhänsli, R., Wagner, T. & Shuwen, D. (2001). Eclogite-facies quartz veins within metabasites of the Dabie Shan (eastern China): Pressure–temperature–time–deformation path, composition of the fluid phase and fluid flow during exhumation of high-pressure rocks. *Contributions to Mineralogy and Petrology* **141(3)**, 322–346.

Fryer, P. (1992). A synthesis of Leg 125 drilling of serpentine seamounts on the Mariana and Izu–Bonin forearcs. *Proceedings of the Ocean Drilling Program, Scientific Results* **125**, 593–614.

Fryer, P., Pearce, J. A., Stokking, L. B. *et al.* (1992). A synthesis of serpentinites seamounts on the Mariana and Izu-Bonin forearcs. *Proceedings of the Ocean Drilling Program, Scientific Results* **125**, 593–614.

Fusseis, F., Regenauer-Lieb, K., Liu, J., Hough, R. M. & De Carlo, F. (2009). Creep cavitation can establish a dynamic granular fluid pump in ductile shear zones. *Nature* **459(7249)**, 974–977.

Gao, J. & Klemd, R. (2001). Primary fluids entrapped at blueschist to eclogite transition: Evidence from the Tianshan meta-subduction complex in northwestern China. *Contributions to Mineralogy and Petrology* **142(1)**, 1–14.

Giorgis, D., Cosca, M. & Li, S. (2000). Distribution and significance of extraneous argon in UHP eclogite (Sulu Terrain, China): Insight from *in situ* $^{40}Ar/^{39}Ar$ UV-laser ablation analysis. *Earth and Planetary Science Letters* **181**, 601–615.

Gosso, G., Dal Piaz, G. V., Piovano, V. & Polino, R. (1979). High pressure emplacement of early-Alpine nappes, post-nappe deformations and structural levels (internal northwestern Alps). *Memorie degli Instituti di Geologia e Mineralogia della Universita di Padova* **32**, 5–15.

Green, E. C. R., Holland, T. J. B. & Powell, R. (2007). An order–disorder model for omphacite pyroxenes in the system jadeite–diopside–hedenbergite–acmite with applications to eclogitic rocks. *American Mineralogist* **92**, 1181–1189.

Groome, W. G., Johnson, S. E. & Koons, P. O. (2006). The effects of porphyroblast growth on the effective viscosity of metapelitic rocks: Implications for the strength of the middle crust. *Journal of Metamorphic Geology* **24(5)**, 389–407.

Hacker, B. R., Peacock, S. M., Abers, G. A. & Holloway, S. D. (2003). Subduction factory—2. Are intermediate-depth earthquakes in subducting slabs linked to metamorphic dehydration reactions? *Journal of Geophysical Research—Solid Earth* **108 (B1)**, doi:10.1029/2001JB001129.

Handy, M. R. & Oberhänsli, R. (2004). Age map of the metamorphic structure of the Alps—tectonic interpretation and outstanding problems. *Mitteilungen der Österreichischen Mineralogischen Gesellschaft* **149**, 97–121.

Hippertt, J. F. M. (1994). Grain boundary microstructures in micaceous quartzite: Significance for fluid movement and deformation processes in low metamorphic shear zones. *Journal of Geology* **102**, 331–348.

Holness, M. B. (1993). Temperature and pressure dependence of quartz–aqueous fluid dihedral angles: The control of adsorbed H_2O on the permeability of quartzites. *Earth and Planetary Science Letters* **117(3–4)**, 363–377.

Iwamori, H. (1998). Transportation of H_2O and melting in subduction zones. *Earth and Planetary Science Letters* **160(1–2)**, 65–80.

Jamtveit, B., Malthe-S&cslash;renssen, A. & Kostenko, O. (2008). Reaction enhanced permeability during retrogressive metamorphism. *Earth and Planetary Science Letters* **267(3–4)**, 620–627.

John, T. & Schenk, V. (2003). Partial eclogitisation of gabbroic rocks in a late Precambrian subduction zone (Zambia): Prograde metamorphism triggered by fluid infiltration. *Contributions to Mineralogy and Petrology* **146(2)**, 174–191.

Keller, L. M., Abart, R., Wirth, R., Schmid, D. W. & Kunze, K. (2006). Enhanced mass transfer through short-circuit diffusion: Growth of garnet reaction rims at eclogite facies conditions. *American Mineralogist* **91(7)**, 1024–1038.

Kessel, R., Schmidt, M. W., Ulmer, P. & Pettke, T. (2005). Trace element signature of subduction-zone fluids, melts and supercritical liquids at 120–180 km depth. *Nature* **437(7059)**, 724–727.

Konrad-Schmolke, M., Handy, M. R., Babist, J. & O'Brien, P. J. (2005). Thermodynamic modelling of diffusion-controlled garnet growth. *Contributions to Mineralogy and Petrology* **149(2)**, 181–195.

Konrad-Schmolke, M., Babist, J., Handy, M. R. & O'Brien, P. J. (2006). The physico-chemical properties of a subducted slab from garnet zonation patterns (Sesia Zone, Western Alps). *Journal of Petrology* **47(11)**, 2123–2148.

Konrad-Schmolke, M., O'Brien, P. J. & Heidelbach, F. (2007). Compositional re-equilibration of garnet: The importance of sub-grain boundaries. *European Journal of Mineralogy* **19(4)**, 431–438.

Konrad-Schmolke, M., Zack, T., O'Brien, P. J. & Jacob, D. E. (2008*a*). Combined thermodynamic and rare earth element modelling of garnet growth during subduction: Examples from ultrahigh-pressure eclogite of the Western Gneiss Region, Norway. *Earth and Planetary Science Letters* **272(1–2)**, 488–498.

Konrad-Schmolke, M., O'Brien, P. J., de Capitani, C. & Carswell, D. A. (2008*b*). Garnet growth at high- and ultra-high pressure conditions and the effect of element fractionation on mineral modes and composition. *Lithos* **103(3–4)**, 309–332.

Koons, P. O. (1986). Relative geobarometry from high-pressure rocks of quartzofeldspathic composition from the Sesia Zone, Western Alps, Italy. *Contributions to Mineralogy and Petrology* **93(3)**, 322–334.

Kostenko, O., Jamtveit, B., Austrheim, H., Pollok, K. & Putnis, C. (2002). The mechanism of fluid infiltration in peridotites at Almklovdalen, Western Norway. *Geofluids* **2(3)**, 203–215.

Lardeaux, J.-M. & Spalla, M. I. (1991). From granulites to eclogites in the Sesia zone (Italian Western Alps); a record of the opening and closure of the Piedmont ocean. *Journal of Metamorphic Geology* **9(1)**, 35–59.

Lin, C. H., Huang, B. S. & Rau, R. J. (1999). Seismological evidence for a low-velocity layer within the subducted slab of southern Taiwan. *Earth and Planetary Science Letters* **174(1–2)**, 231–240.

Lundstrom, C. C. (2000). Rapid diffusive infiltration of sodium into partially molten peridotite. *Nature* **403(6769)**, 527–530.

Mancktelow, N. S. & Pennacchioni, G. (2004). The influence of grain boundary fluids on the microstructure of quartz–feldspar mylonites. *Journal of Structural Geology* **26(1)**, 47–69.

Manning, C. E. (2004). The chemistry of subduction-zone fluids. *Earth and Planetary Science Letters* **223(1–2)**, 1–16.

Marmo, B. A., Clarke, G. L. & Powell, R. (2002). Fractionation of bulk-rock composition due to porphyroblast growth: Effects on eclogite facies mineral equilibria, Pam Peninsula, New Caledonia. *Journal of Metamorphic Geology* **20(1)**, 151–165.

Marschall, H. R., Ludwig, T., Altherr, R., Kalt, A. & Tonarini, S. (2006). Syros metasomatic tourmaline: Evidence for very high-$\delta^{11}B$ fluids in subduction zones. *Journal of Petrology* **47(10)**, 1915–1942.

Milke, R. & Wirth, R. (2003). The formation of columnar fibre texture in wollastonite rims by induced stress and implications for diffusion-controlled corona growth. *Physics and Chemistry of Minerals* **30**, 230–242.

Mukherjee, B. K., Sachan, H. K., Ogasawara, Y., Muko, A. & Yoshioka, N. (2003). Carbonate-bearing UHPM rocks from the Tso-Morari region, Ladakh, India: Petrological implications. *International Geology Review* **45**, 49–69.

Nakamura, M. & Watson, E. B. (2001). Experimental study of aqueous fluid infiltration into quartzite: Implications for the kinetics of fluid redistribution and grain growth driven by interfacial energy reduction. *Geofluids* **1(2)**, 73–89.

Oliver, N. H. S. (1996). Review and classification of structural controls on fluid flow during regional metamorphism. *Journal of Metamorphic Geology* **14(4)**, 477–492.

Oliver, N. H. S. & Bons, P. D. (2001). Mechanisms of fluid flow and fluid–rock interaction in fossil metamorphic hydrothermal systems inferred from vein–wallrock patterns, geometry and microstructure. *Geofluids* **1(2)**, 137–162.

Peacock, S. M. (1987). Serpentinization and infiltration metasomatism in the Trinity peridotite, Klamath Province, northern California: Implications for subduction zones. *Contributions to Mineralogy and Petrology* **95(1)**, 55–70.

Penniston-Dorland, S. C., Sorensen, S. S., Ash, R. D. & Khadke, S. V. (2010). Lithium isotopes as a tracer of fluids in a subduction zone mélange: Franciscan complex, CA. *Earth and Planetary Science Letters* **292(1–2)**, 181–190.

Philippot, P. & Selverstone, J. (1991). Trace element-rich brines in eclogitic veins: implications for fluid composition and transport during subduction. *Contributions to Mineralogy and Petrology* **106**, 417–430.

Pognante, U. (1989). Tectonic implications of lawsonite formation in the Sesia zone (Western Alps). *Tectonophysics* **162(3–4)**, 219–227.

Poli, S. & Schmidt, M. W. (1997). The high-pressure stability of hydrous phases in orogenic belts: An experimental approach on eclogite-forming processes. *Tectonophysics* **273(1–2)**, 169–184.

Putnis, A. (2002). Mineral replacement reactions: From macroscopic observations to microscopic mechanisms. *Mineralogical Magazine* **66(5)**, 689–708.

Rosenbaum, G., Giles, D., Saxon, M., Betts, P. G., Weinberg, R. F. & Duboz, C. (2005). Subduction of the Nazca Ridge and the Inca Plateau: Insights into the formation of ore deposits in Peru. *Earth and Planetary Science Letters* **239(1)**, 18–32.

Rubatto, D., Gebauer, D. & Compagnoni, R. (1999). Dating of eclogite facies zircons: the age of Alpine metamorphism in the Sesia–Lanzo Zone (Western Alps). *Earth and Planterary Science Letters* **167**, 141–158.

Rubie, D. C. (1983). Reaction-enhanced ductility: The role of solid–solid univariant reactions in deformation of the crust and mantle. *Tectonophysics* **96(3–4)**, 331–352.

Rubie, D. C. (1986). The catalysis of mineral reactions by water and restrictions on the presence of aqueous fluid during metamorphism. *Mineralogical Magazine* **50**, 399–415.

Ryan, J. G., Morris, J., Tèra, F., Leeman, W. P. & Tsvetkov, A. (1995). Cross-arc geochemical variations in the Kurile arc as a function of slab depth. *Science* **270(5236)**, 625–627.

Scambelluri, M. & Philippot, P. (2001). Deep fluids in subduction zones. *Lithos* **55(1–4)**, 213–227.

Schmid, S. M. & Kissling, E. (2000). The arc of the western Alps in the light of geophysical data on deep crustal structures. *Tectonics* **19(1)**, 62–85.

Schmidt, M. W. & Poli, S. (1998). Experimentally based water budgets for dehydrating slabs and consequences for arc magma generation. *Earth and Planetary Science Letters* **163(1–4)**, 361–379.

Schulte, B. & Sindern, S. (2002). K-rich fluid metasomatism at high-pressure metamorphic conditions: Lawsonite decomposition in rodingitized ultramafite of the Maksyutovo Complex, Southern Urals (Russia). *Journal of Metamorphic Geology* **20(6)**, 529–541.

Sorensen, S. S. (1988). Petrology of amphibolite-facies mafic and ultramafic rocks from the Catalina schist, southern California: Metasomatism and migmatization in a subduction zone metamorphic setting. *Journal of Metamorphic Geology* **6(4)**, 405–435.

Sorensen, S. S., Grossman, J. N. & Perfit, M. R. (1997). Phengite-hosted LILE enrichment in eclogite and related rocks: Implications for fluid-mediated mass transfer in subduction zones and arc magma genesis. *Journal of Petrology* **38(1)**, 3–34.

Spandler, C., Mavrogenes, J. & Hermann, J. (2007). Experimental constraints on element mobility from subducted sediments using high-P synthetic fluid/melt inclusions. *Chemical Geology* **239**, 228–249.

Spandler, C., Hermann, J. R., Arculus, R. & Mavrogenes, J. (2003). Redistribution of trace elements during prograde metamorphism from lawsonite blueschist to eclogite facies; implications for deep subduction-zone processes. *Contributions to Mineralogy and Petrology* **146(2)**, 205–222.

St-Onge, M. R. & Lucas, S. B. (1995). Large-scale fluid infiltration, metasomatism and re-equilibration of Archean basement granulites during palaeoproterozoic thrust belt construction, Ungava Orogen, Canada. *Journal of Metamorphic Geology* **13(4)**, 509–535.

Stünitz, H. (1989). , Partitioning of metamorphism and deformation in the boundary region of the 'Seconda Zona Diorito-Kinzigitica', Sesia Zone, Western Alps. PhD thesis, Swiss Federal Institute of Technology, Zurich, 244 pp.

Tropper, P., Essene, E. J., Sharp, Z. D. & Hunziker, J. C. (1999). Application of K-feldspar–jadeite–quartz barometry to eclogite facies metagranites and metapelites in the Sesia Lanzo Zone (Western Alps, Italy). *Journal of Metamorphic Geology* **17(2)**, 195–209.

van der Straaten, F., Schenk, V., John, T. & Gao, J. (2008). Blueschist-facies rehydration of eclogites (Tian Shan, NW China): Implications for fluid–rock interaction in the subduction channel. *Chemical Geology* **255(1–2)**, 195–219.

Venturini, G. (1995). , Geology, geochemistry and geochronology of the inner central Sesia Zone (Western Alps, Italy). PhD Thesis, Université de Lausanne.

Wain, A. (1997). New evidence for coesite in eclogite and gneisses: Defining an ultrahigh-pressure province in the Western Gneiss region of Norway. *Geology* **25(10)**, 927–930.

Xia, S., Zhao, D. & Qui, X. (2008). Tomographic evidence for the subducting oceanic crust and forearc mantle serpentinization under Kyushu, Japan. *Tectonophysics* **449**, 85–96.

Zack, T. & John, T. (2007). An evaluation of reactive fluid flow and trace element mobility in subducting slabs. *Chemical Geology* **239(3–4)**, 199–216.

Zucali, M., Spalla, M. I. & Gosso, G. (2002). Strain partitioning and fabric evolution as a correlation tool: The example of the Eclogitic Micaschists complex in the Sesia–Lanzo Zone (Monte Mucrone–Monte Mars, Western Alps, Italy). *Schweizerische Mineralogische und Petrographische Mitteilungen* **82(3)**, 429–454.